DOE/NASA/0008-80/11
NASA CR-159854

(NASA-CR-159854) REGENERATOR MATRIX PHYSICAL PROPERTY DATA (Ford Motor Co.) 51 p HC A04/MF A01 CSCL 05A

N80-30228

Unclas
G3/85 28459

REGENERATOR MATRIX PHYSICAL PROPERTY DATA

C. A. Fucinari
Research Staff
Ford Motor Co.

MAY 1980

Prepared for
NATIONAL AERONAUTICS AND SPACE ADMINISTRATION
Lewis Research Center
Under Contract DEN 3-8

For
U.S. DEPARTMENT OF ENERGY
Conservation and Solar Energy
Office of Transportation Programs

NOTICE

DOE/NASA/0008-80/11
NASA CR-159854

REGENERATOR MATRIX PHYSICAL PROPERTY DATA

C. A. Fucinari
Research Staff
Ford Motor Co.

MAY, 1980

Prepared for
National Aeronautics and Space Administration
Lewis Research Center
Cleveland, Ohio 44135
Under Contract DEN 3-8

For
U.S. DEPARTMENT OF ENERGY
Conservation and Solar Energy
Office of Transportation Programs
Washington D.C. 20545
Under Interagency Agreement EC-77-A-31-1044

TABLE OF CONTENTS

Page No.

LIST OF ILLUSTRATIONS

LIST OF ILLUSTRATIONS

LIST OF TABLES

SUMMARY

In order to arrive at an optimum regenerator design for a given application the matrix fin geometries being considered must be completely characterized. Regenerator performance and durability, which are two diverse design areas, are both highly dependent on the matrix fin geometry selected.

Based on the extensive engine durability testing at 800°C (1472°F) and 1000°C (1832°F) in the Ford 707 gas turbine engine, the three most promising regenerator matrix materials have been completely characterized. This report summarizes the important design parameters for these matrices in the following categories:

Aero-Thermodynamic Properties — The standard and an alternate form of performance characteristics allow the designer to estimate performance for a fixed size exchanger or to determine the size required to attain specified performance objectives.

Matrix Physical Properties — Thermal expansion, modulus of elasticity and modulus of rupture are the important parameters required to estimate the thermal stress capacity of a given design for specified operating conditions.

Resistance to Chemical Attack — Once the regenerator is designed properly to have sufficient thermal stress capacity, the matrix material must be resistant to the exposure of corrosive agents such as sulphuric acid in the engine exhaust or the presence of sodium in the inlet air or fuel system.

Thermal Stability — The upper temperature limit of the matrix material must be determined to ensure dimensional stability will be acceptable. Excessive dimensional change can lower the thermal stress capacity of a given design.

INTRODUCTION

An optimum ceramic regenerator design requires an effective compromise between thermal and mechanical stress capability combined with aero-thermodynamic performance potential. Even though regenerator stress and performance are two diverse design areas, they are both highly dependent on the matrix fin geometry selected.

Since 1974, Ford Motor Company has evaluated several cellular ceramic structures, which were manufactured by various suppliers, for regenerator application in the Ford 707 gas turbine engine. Test samples and full-size cores have been evaluated in the laboratory and 707 engine, respectively. From 1974 through 1979, this development program was supported on a cost sharing basis by EPA, ERDA and DOE/NASA. The results have been documented in references 1 thru 3.

Based on these results, the following three matrices have the best potential for achieving durability and performance objectives for use in gas turbine engines, Stirling engines and waste heat recovery systems.

1. An aluminum-silicate (AS) sinusoidal flow passage made from a corrugated wet paper process by Supplier A.

2. An extruded isosceles triangle flow passage from a MAS material from Supplier I.

3. A second generation MAS matrix incorporating a square flow passage formed by an embossing process by Supplier D.

This report will document the pertinent matrix parameters required for aero-thermodynamic performance, physical properties that influence mechanical and thermal durability, resistance to chemical attack and thermal stability for each of these matrices.

DISCUSSION OF RESULTS

1.0 AERO-THERMODYNAMIC PROPERTIES

The matrix characteristics which affect regenerator performance are the ability to transfer heat effectively to and from the working fluids, to store heat in the matrix with little conductance loss, and to perform these functions with a minimum fluid pressure drop across the matrix. A measure of the heat transfer characteristics is the Colburn Number (J) and Fanning Friction Factor (F) indicates the pressure drop characteristics of the matrix. Both of these dimensionless parameters are a function of Reynold's Number (RE) for a given matrix geometry.

In order to obtain the basic heat transfer and pressure drop data, a shuttle rig similar to the "sliding drawer" technique described in Reference 4 was used. The shuttle rig, shown in Figure 1.1 consists of two concentric cylinders fabricated from

a material with extremely low thermal conductivity (acrylic plastic). The outer cylinder (Figure 1.2) consists of four square ports 90° apart, which contain pressure taps and thermocouples. The inner cylinder (Figure 1.3), which contains the matrix sample, is mechanically rotated 90° between the hot and cold air streams. The tight clearance between the concentric cylinders prevents the air from leaking from one stream to the other.

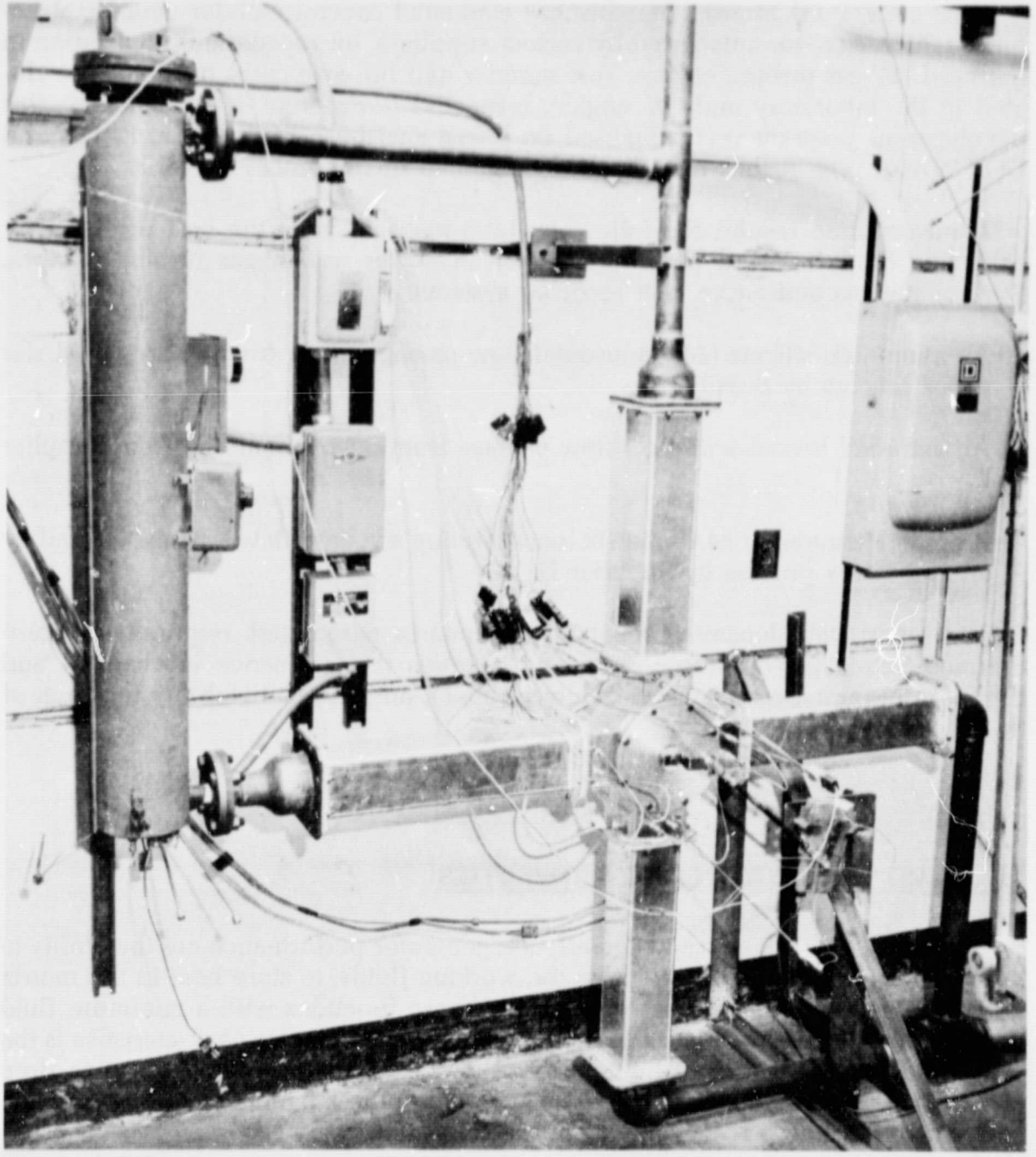

Figure 1.1 — Photograph of Shuttle Rig

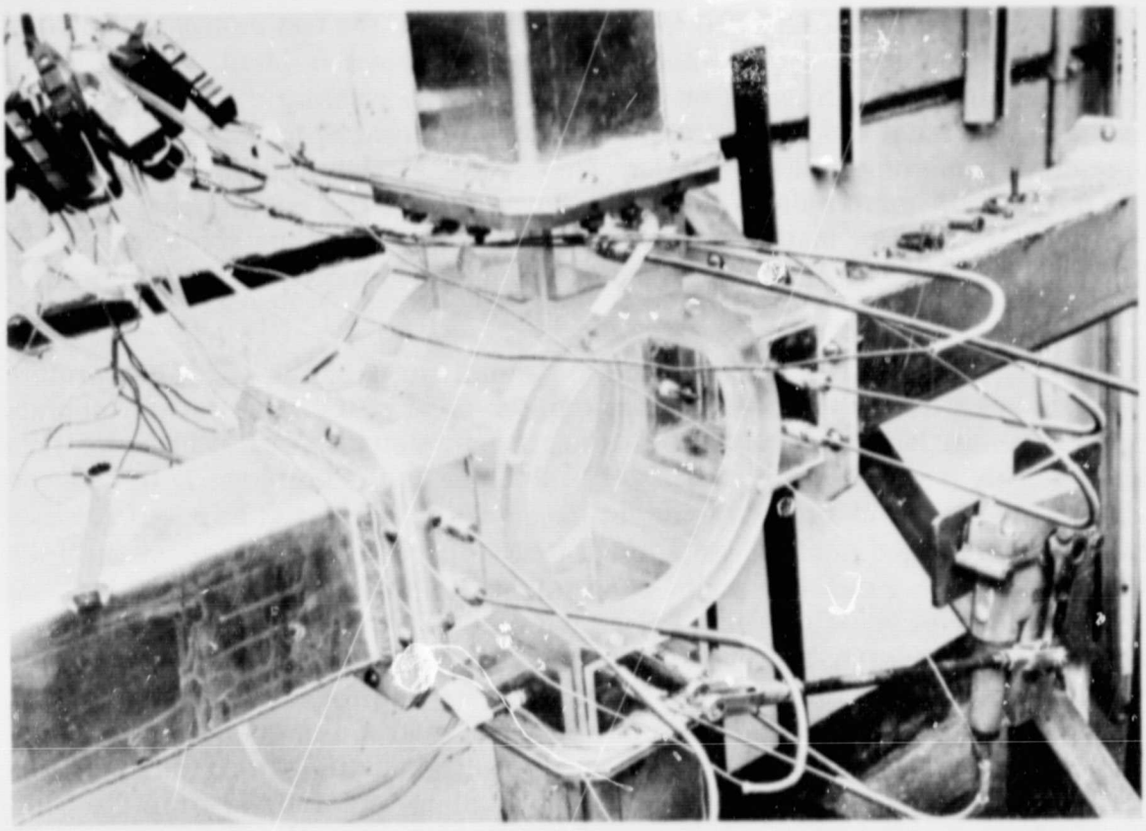

Figure 1.2 — Photograph of Outer Cylinder Used in the Shuttle Rig

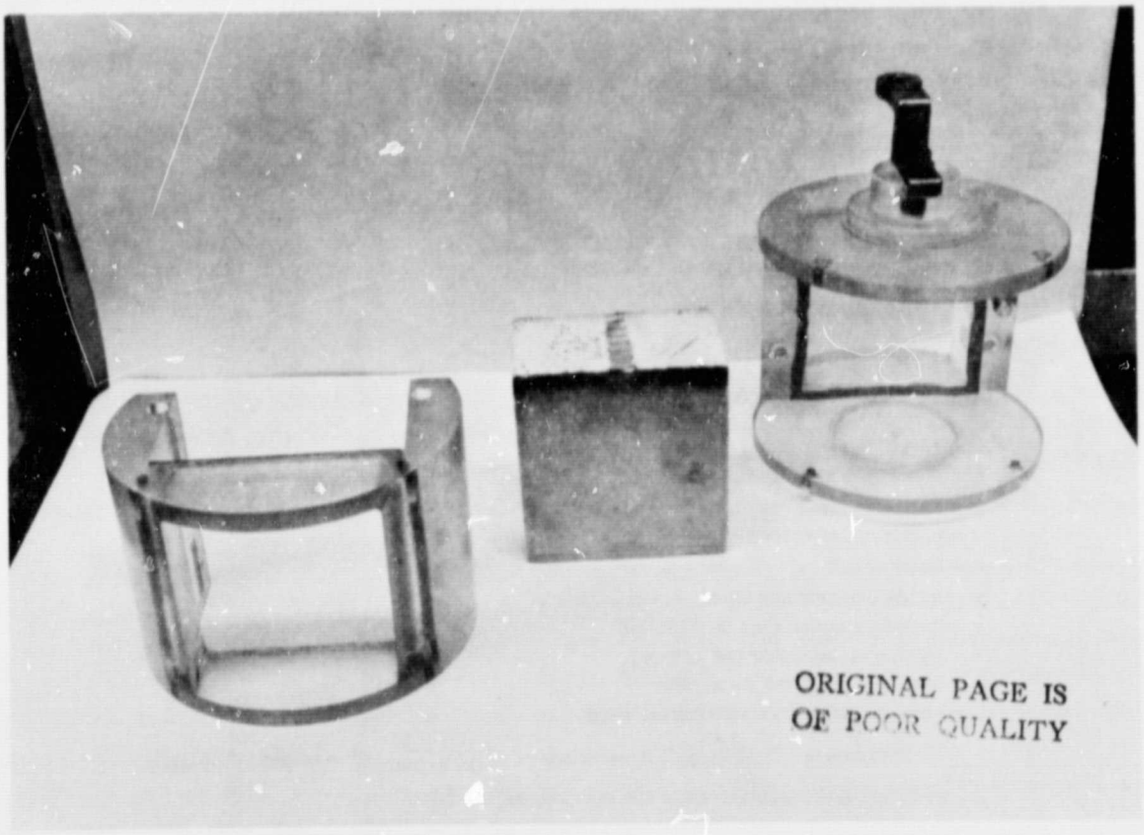

Figure 1.3 — Photograph of Inner Cylinder Used in the Shuttle Rig

With the inner cylinder exposed to the hot air stream, the test matrix is heated to a uniform temperature of approximately 12°C (22°F) above ambient. A step change in fluid temperature is imposed on the test matrix by rotating the inner cylinder 90°. The downstream fluid temperature, which is referenced to the upstream fluid temperature, is monitored and recorded versus time. By determining the maximum slope of the fluid temperature difference curve during the cooling transient, the Colburn No. of the test matrix can be determined for each flow condition (Reynold's No.). The theoretical basis for this measurement technique is described in Reference 4.

In addition to the dependence on the maximum slope of the fluid temperature difference curve during the cooling transient, the level of the heat transfer characteristics (Colburn No.) is dependent on the fin parameter values utilized for data reduction. This was previously discussed in Section Q of Reference 1. In order to determine the pertinent fin configuration parameters (Figure 1.4) required for data reduction, an enlarged photo (Figure 1.5) of a 25.4 mm (1 inch) square section of the test matrix is taken. From this photo the number of openings per row per inch (X) and the number of rows per inch (Y) is determined. A computer program determines the open area (σ), hydraulic diameter (DH), and heat transfer surface area per unit volume (β) as a function of X, Y, fillet radius, and fin material thickness (S). After measuring the weight and volume of the test matrix, the open area (σ) is determined based on the wall density (ρW) of the matrix material. Once the open area is established, the remaining parameters (DH, β, S) are determined from the computer read-out for the X, Y, and S combination. Consequently, the pertinent fin parameters required (σ and DH) for data reduction are highly dependent on the accuracy of the wall density (ρW) value of the matrix material.

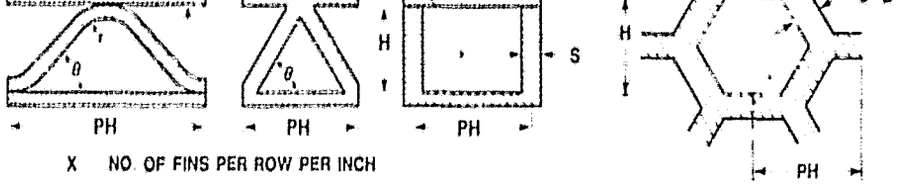

X = NO. OF FINS PER ROW PER INCH

Y = NO. OF ROWS PER INCH

H = FIN HEIGHT = $\frac{1}{Y}$ − B

PH = FIN PITCH = $(\frac{1}{X})$ RECTANGULAR OR HEXAGONAL = $(\frac{2}{X})$ TRIANGULAR

A.R. = ASPECT RATIO = PH / H

B = PLATE THICKNESS

S = FIN THICKNESS

r = RADIUS OF CURVATURE

θ = SHAPE ANGLE

N = NO. OF OPENINGS PER SQ. IN.

A_Δ = CROSS-SECTIONAL AREA OF 1 OPENING

WP = WETTED PERIMETER OF ONE OPENING

DH = HYDRAULIC DIAMETER = $4 A_\Delta$ / W.P.

σ = RATIO OF OPEN AREA TO FRONTAL AREA

σ TRIANGULAR = $\frac{2A_\Delta}{PH\,(H+B)}$ σ RECTANGULAR = $\frac{H\,(PH-S)}{(H+B)\,(PH)}$ σ HEXAGONAL = $\frac{H^2}{(H+B)^2}$

β = HEAT TRANSFER SURFACE AREA PER UNIT VOLUME = $\frac{4\sigma}{DH}$

Figure 1.4 — Definition of Fin Parameters

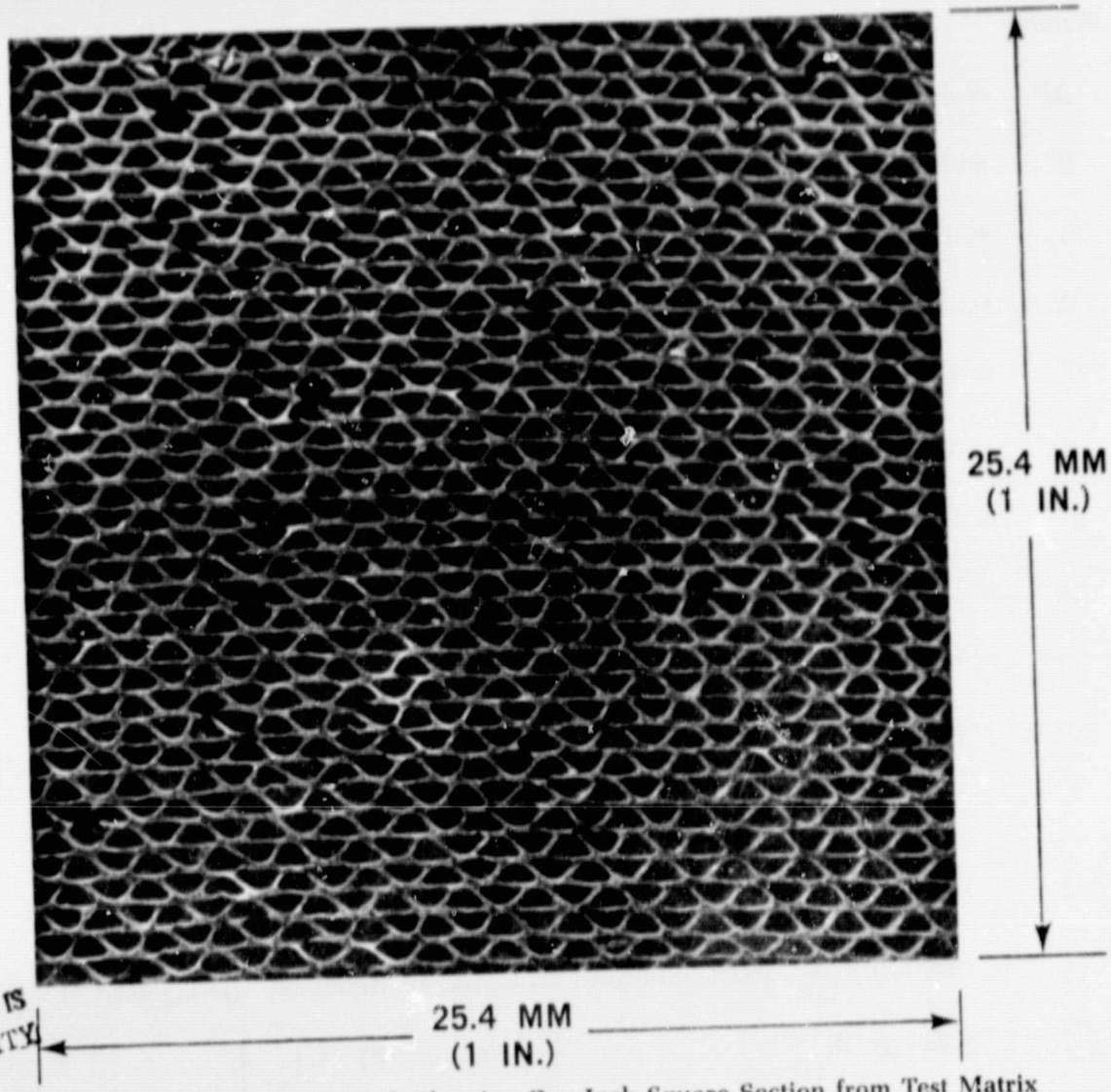

Figure 1.5 — Photograph Showing One-Inch Square Section from Test Matrix

Since erroneous estimates of the fin parameters (σ and DH) can introduce significant discrepancies in the F and J curves, an alternate set of heat transfer and pressure drop characteristics that eliminates the necessity of estimating fin parameters were derived (Section Q.6 of Reference 1). In addition, the alternate characteristics allow a direct comparison of test data from different sources, since a universal method of determining pertinent fin parameters is non-existent at this time. The alternate pressure drop and heat transfer characteristics can be expressed in the following forms:

$$\frac{\Delta P \cdot P}{L} = C \frac{\dot{W}^{1.673} T}{A_F}$$

$$\frac{NTU}{L} = A \left[\frac{A_F T^{.673}}{\dot{W}} \right]^{-X_2}$$

Where:

ΔP = Matrix pressure drop — KPa (PSI)

P = Fluid pressure — KPa (PSIA)

L = Flow length — CM. (In.)

W = Air Mass flow rate — Kg/Sec. (Lb./Sec.)

T = Fluid temperature — °K. (°R.)

A_F = Matrix frontal area — $M.^2$ ($FT.^2$)

σ = Open area ratio

C_1 = Fanning Friction Factor constant for laminar flow = F·RE

DH = Hydraulic diameter — CM. (In.)

NTU = By definition the number of heat transfer units (determined from the maximum slope of the fluid temperature difference curve during the cooling transient as described in Reference 4)

C_2 = Colburn No. constant for laminar flow = J/RE^{X_2}

X_2 = Reynold's No. (RE) exponent from the Colburn No. ($J=C_2\ RE^{X_2}$)

$$C = 3.56\ (10^{-9})\frac{C_1}{\sigma DH^2} \qquad \left[3.506\ (10^{-10})\frac{C_1}{\sigma DH^2}\right]$$

$$A = 4.98\left[62.6(10^{-7})\right]^{-X_2}\left(\frac{C_2\sigma}{DH\ (1-X_2)}\right)^{-X_2} \qquad \left[4.98\left[21.9(10^{-7})\right]^{-X_2}\left(\frac{C_2\sigma}{DH\ (1-X_2)}\right)^{-X_2}\right]$$

If $X_2 = -1$; then:

$$A = 3.11\ (10^{-5})\frac{C_2\sigma}{DH^2} \qquad \left[1.09\ (10^{-5})\frac{C_2\sigma}{DH^2}\right]$$

Once the constants (C and A) have been determined from the equation of the line for the alternate performance characteristics, the pertinent constants (C_1 and C_2) for the basic performance characteristics can be determined from estimated values of σ and DH.

A description of the three matrix geometries that are characterized in this report are as follows:

1. Matrix No. 1 — Supplier A produced the sinusoidal structure (Figure 1.6) by the corrugated wet paper process using aluminum-silicate (A-S) material (.061 mm thick).

2. Matrix No. 2 — Supplier I extruded the isosceles triangular configuration (Figure 1.7) using a magnesium-aluminum-silicate (M-A-S) material (.135 mm thick).

3. Matrix No. 3 — The essentially square matrix (Figure 1.8) was formed by the embossing process by Supplier D with a second generation M-A-S material (.193 mm thick).

The standard heat transfer (J) and pressure drop (F) characteristics for these matrices, which depend on the values determined for open area ratio (σ) and hydraulic diameter (DH), are illustrated on Figure 1.9. These characteristics are based on the actual geometric opening with the wall material thickness factored out. The pertinent matrix parameters required for performance evaluation are listed in Table 1.1.

The alternate heat transfer (NTU/L) and pressure drop ($\Delta P \cdot P/L$) characteristics for these matrices, which are based on measured test data, are illustrated on Figure 1.10.

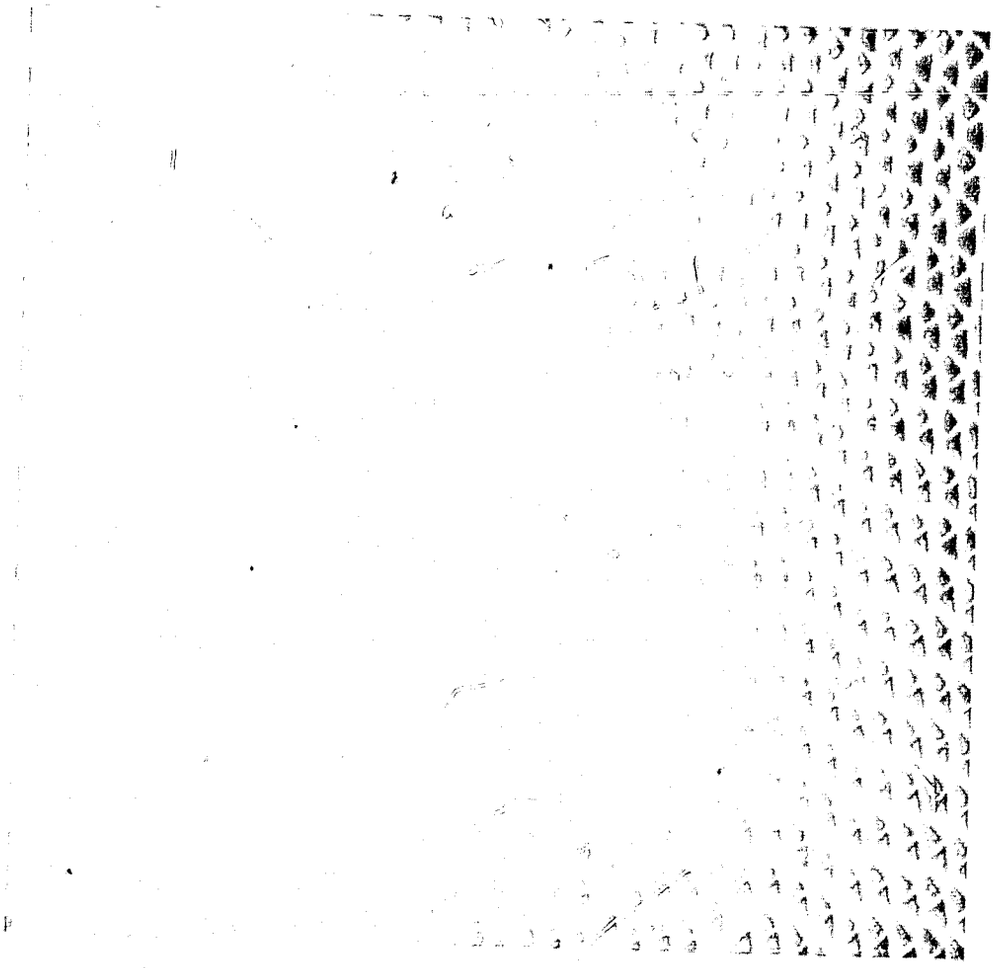

Figure 1.6 — Photograph Showing Section from Supplier A Wrapped Sinusoidal Structure Fabricated with A-S Material (.061 mm Thick).

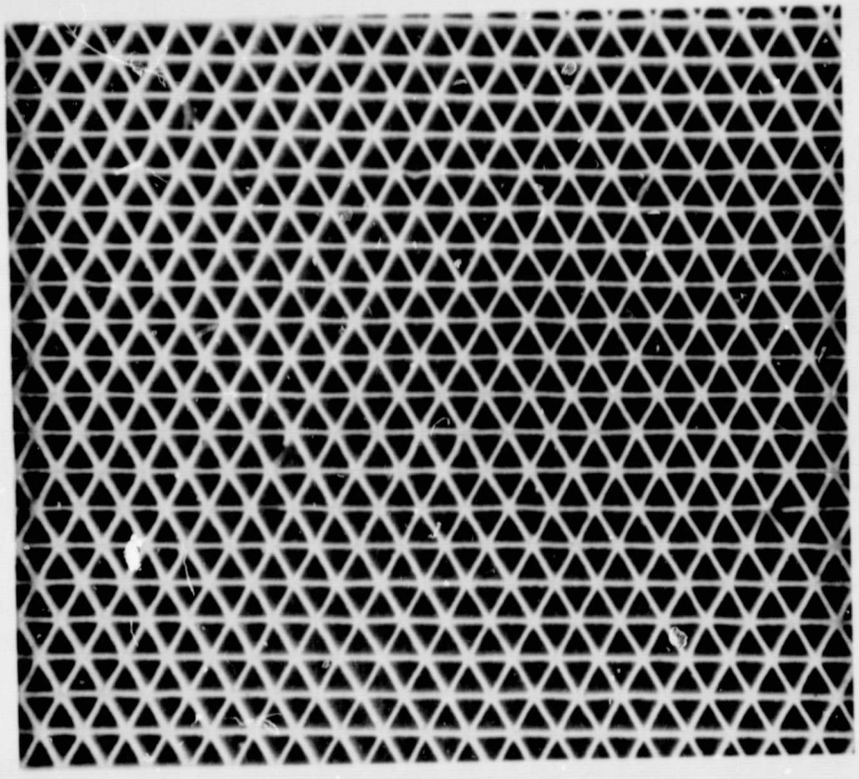

Figure 1.7 — Photograph Showing Section from Supplier I Extruded Isosceles Triangular Structure Fabricated with MAS Material (.135 mm Thick).

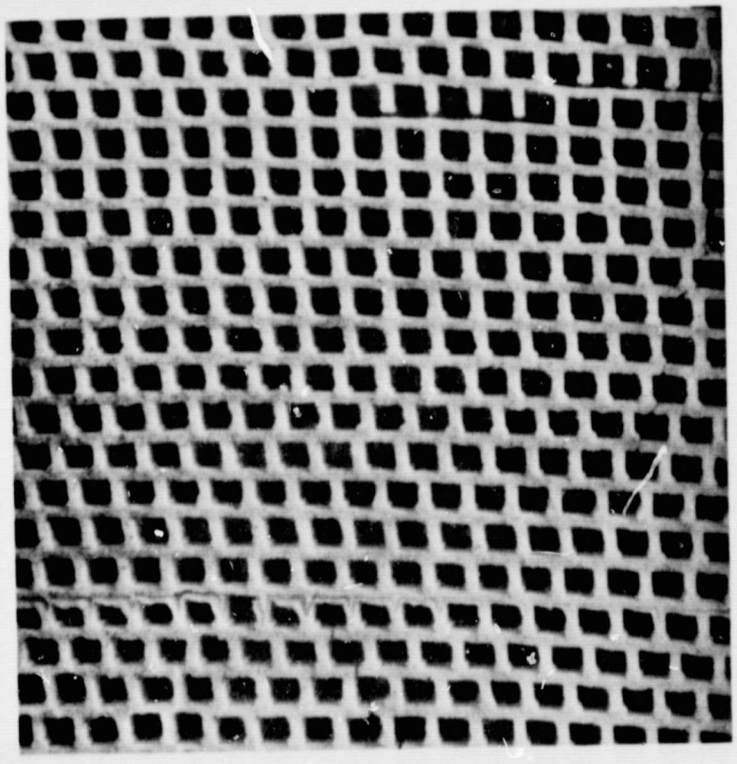

Figure 1.8 — Photograph Showing Section from Supplier D Embossed Square Structure Fabricated with MAS Material (.193 mm Thick).

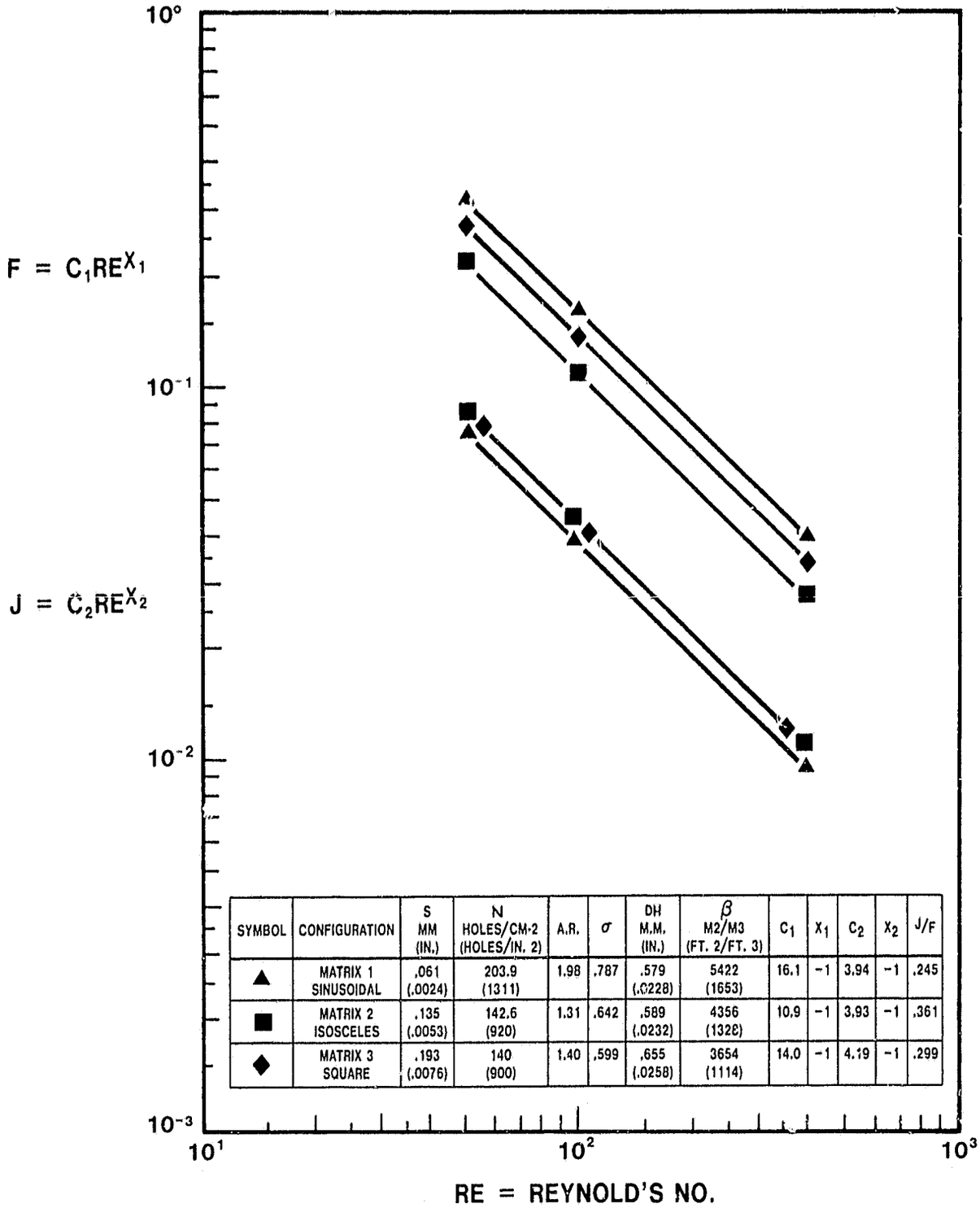

SYMBOL	CONFIGURATION	S MM (IN.)	N HOLES/CM-2 (HOLES/IN. 2)	A.R.	σ	DH M.M. (IN.)	β M2/M3 (FT. 2/FT. 3)	C_1	X_1	C_2	X_2	J/F
▲	MATRIX 1 SINUSOIDAL	.061 (.0024)	203.9 (1311)	1.98	.787	.579 (.0228)	5422 (1653)	16.1	−1	3.94	−1	.245
■	MATRIX 2 ISOSCELES	.135 (.0053)	142.6 (920)	1.31	.642	.589 (.0232)	4356 (1328)	10.9	−1	3.93	−1	.361
◆	MATRIX 3 SQUARE	.193 (.0076)	140 (900)	1.40	.599	.655 (.0258)	3654 (1114)	14.0	−1	4.19	−1	.299

Figure 1.9 — Standard Aero-Thermodynamic Performance Characteristics for Matrices 1, 2, and 3.

CODE:

R — RECTANGULAR
I.T. — ISOSCELES TRIANGULAR
S.T. — SINUSOIDAL TRIANGULAR
H — HEXAGONAL

$$F = C_1 RE^{X_1}$$

$$J = C_2 RE^{X_2}$$

$$\frac{\Delta P \cdot P}{L} = C \frac{WT^{1.673}}{A_F}$$

$$\frac{NTU}{L} = A \left[\frac{A_{FT}}{W}^{0.673}\right]^{-X2}$$

CORE NO.	SUP-PLIER	TYPE OF FIN	X FINS / CM. (FINS/IN.)	Y ROWS / CM. (ROWS/IN.)	N HOLES / CM.2 (HOLES/IN.2)	S MM. (IN.)	B MM. (IN.)	H MM. (IN.)	PH MM. (IN.)	A.R. PH/H	ρ_W 0 / CC. (LB./FT.3)	L/DH	σ	DH MM. (IN.)	β M.2/M.3 (FT.2/FT.3)	C_1	X_1	C_2	X_2	JF @ RE=100	C $\times 10^5$	A $\times 10^2$
1	A	S.T.	15.8 (38)	13.6 (34.5)	203.9 (1311)	.061 (.0024)	.061 (.0024)	.676 (.0266)	1.336 (.0526)	1.98	2.10 (131.0)	122	.787	.579 (.0228)	5422 (1653)	16.1	−1	3.94	−1	.245	1.30	6.50
2	I	I.T.	15.8 (40)	9.1 (23)	142.6 (920)	.135 (.0053)	.135 (.0053)	.970 (.0382)	1.270 (.0569)	1.31	1.56 (97.1)	121	.642	.589 (.0232)	4536 (1328)	10.9	−1	3.93	−1	.351	1.11	5.11
3	D	R	11.4 (29)	12.2 (31)	140 (900)	.193 (.0076)	.193 (.0076)	.627 (.0247)	.879 (.0345)	1.40	1.55 (97.0)	107	.599	.655 (.0258)	3654 (1114)	14.0	−1	4.19	−1	.299	1.23	4.11

Table 1.1 — Matrix Performance Parameters

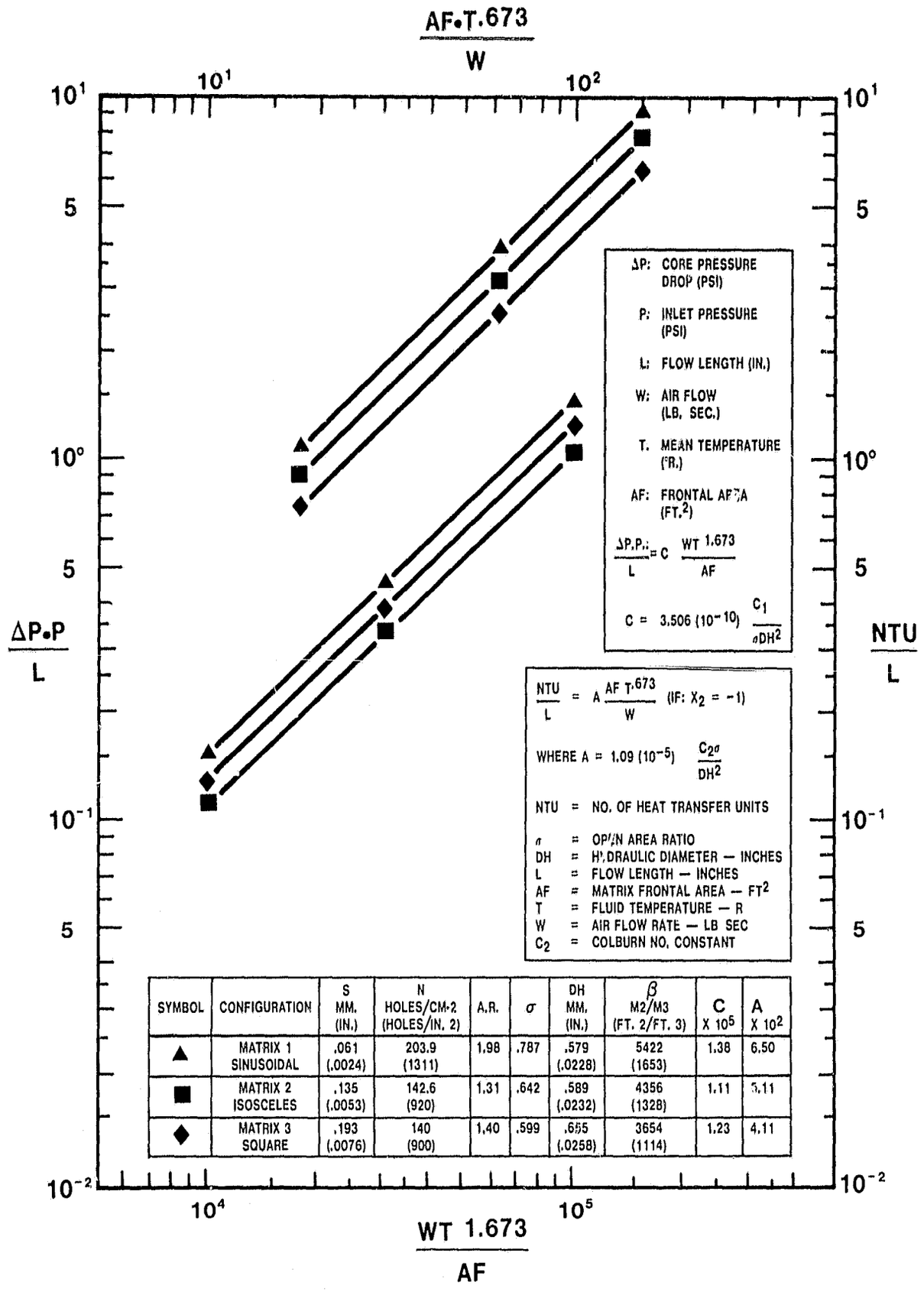

SYMBOL	CONFIGURATION	S MM. (IN.)	N HOLES/CM·2 (HOLES/IN. 2)	A.R.	σ	DH MM. (IN.)	β M2/M3 (FT. 2/FT. 3)	C X 10⁵	A X 10²
▲	MATRIX 1 SINUSOIDAL	.061 (.0024)	203.9 (1311)	1.98	.787	.579 (.0228)	5422 (1653)	1.38	6.50
■	MATRIX 2 ISOSCELES	.135 (.0053)	142.6 (920)	1.31	.642	.589 (.0232)	4356 (1328)	1.11	5.11
◆	MATRIX 3 SQUARE	.193 (.0076)	140 (900)	1.40	.599	.655 (.0258)	3654 (1114)	1.23	4.11

Figure 1.10 — Alternate Aero-Thermodynamic Performance Characteristics for Matrices 1, 2, and 3.

Since the hydraulic diameter of the three matrices are approximately the same, some interesting observations can be made with respect to a fixed size heat exchanger. A gross measure of overall fin efficiency is the ratio of the heat transfer to pressure drop constant for laminar flow ($J/F = C_2/C_1$). From the standard performance characteristics (Figure 1.9), the extruded isosceles triangular structure is the best of the three geometries. The wrapped sinusoidal matrix is the least efficient geometry.

The alternate performance characteristics (Figure 1.10) allow a direct comparison of these fin geometries for a fixed regenerator size at identical flow conditions with the wall thickness and sample uniformity factored in. Based on these characteristics the sinusoidal matrix geometry, which has the minimum wall thickness, would have the highest heat transfer efficiency. This example illustrates the importance of minimizing the wall material thickness.

2.0 MATRIX PHYSICAL PROPERTIES

Matrix physical properties that influence the magnitude of thermal stress in a regenerator core and the ability of the core to withstand thermal and mechanical stress are as follows:

1. Thermal Expansion

2. Modulus of Elasticity (MOE)

3. Modulus of Rupture (MOR)

4. Compressive Strength

These properties were determined by the following techniques:

Thermal expansion is measured using a differential dilatometer. The thermal expansion characteristics for the three matrix geometries selected are illustrated in Figure 2.1.

Modulus of rupture (MOR) and modulus of elasticity (MOE) were measured using a four-point bend test (Figure 2.2). Strain gages are applied to the tensile surface of the 4-point bend specimen and stress versus strain is recorded until specimen failure occurs. The stress application rate is approximately 689 KPa/min. (100 psi/min.) for tangential specimens and approximately 1378 KPa/min. (200 psi/min.) for radial samples.

Compressive strength was measured using 50 mm x 50 mm x 50 mm (2.0 in. x 2.0 in x 2.0 in) specimens loaded to failure in a testing machine at a cross-head speed of 5 mm/min (0.2 in/min). Upper and lower specimen surfaces were ground flat and parallel to ±.025 mm (.001 in). In order to provide uniform loading, thin elastomer sheets were incorporated on the specimen loaded surfaces.

Once the test procedure has been established, proper interpretation of the test data is essential. Typically, the strength of a ceramic material is sensitive to microscopic cracks or flaws such that a number of strength tests on samples of apparently the same material may result in a considerable range of material strengths depending on the size and distribution of the flaws. In addition, the problem is compounded by variations due to the manufacturing process. Variations in cell size and shape, wall material thickness and delaminations associated with the forming and firing stages of the process contribute to the variance in physical properties.

Since there is a considerable amount of scatter associated with these data, a statistical evaluation of matrix physical properties is required. The results of these tests are presented in the form of Weibull distribution plots. The B_{10} and B_{50} values were determined from the Weibull distributions and are tabulated on Table 2.2. A B_{10} value indicates that 10% of the samples will have a smaller value.

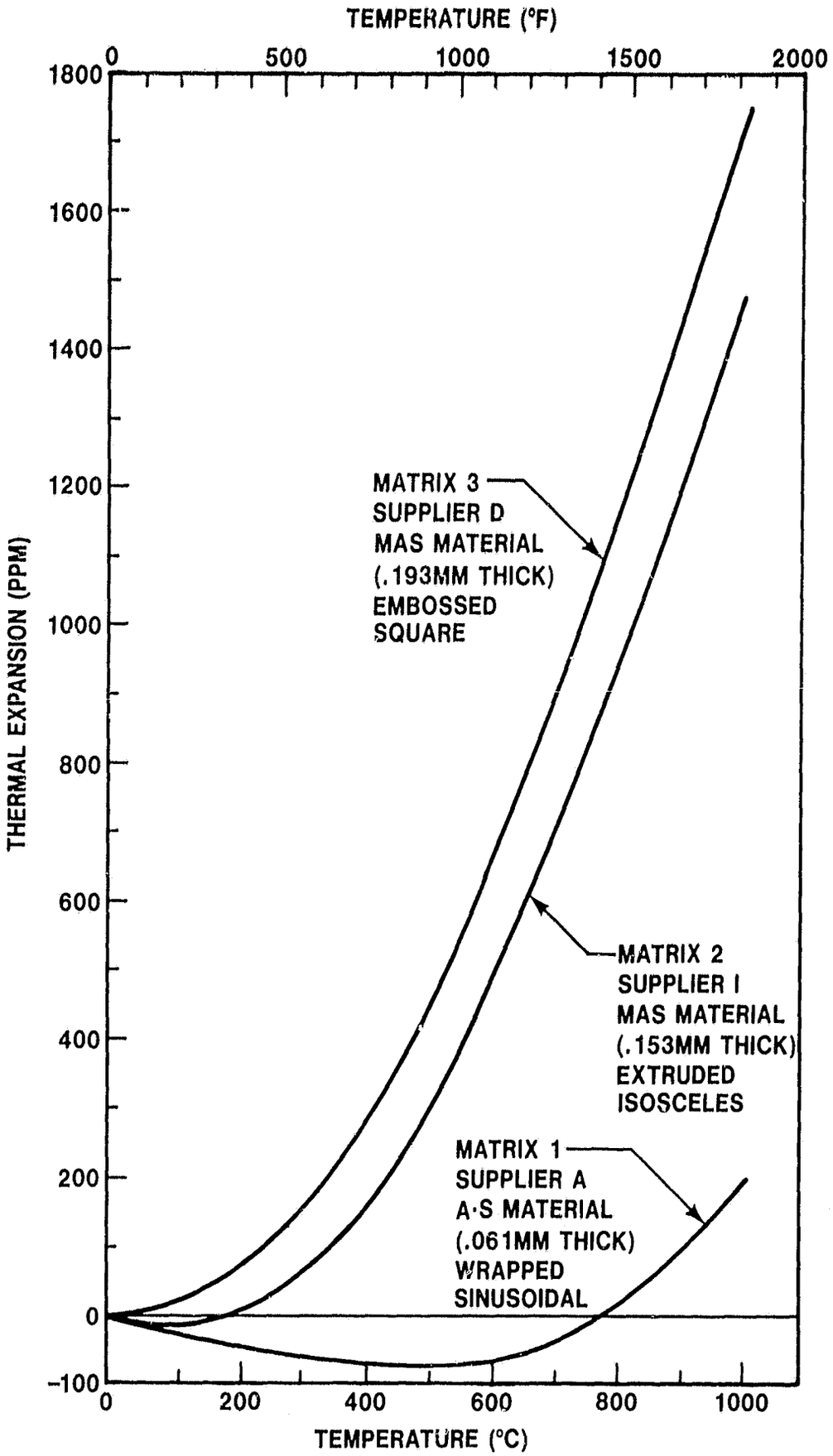

Figure 2.1 — Thermal Expansion Characteristics for Matrices 1, 2 and 3.

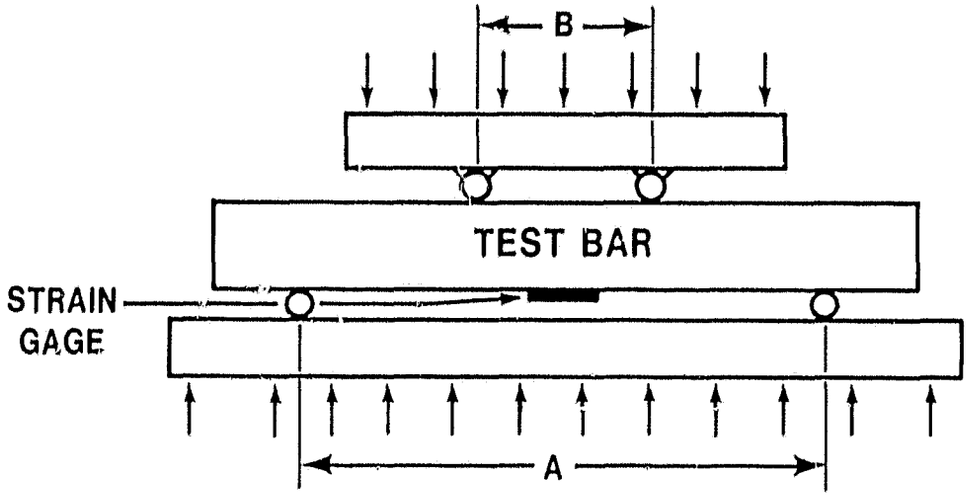

$$\text{STRAIN TOLERANCE} = \frac{\text{BEND STRENGTH (MOR)}}{\text{ELASTIC MODULUS (MOE)}}$$

MATRIX NO.	A	B
1	4.0	2.0
2	1.5	.5
3	3.5	1.5

Figure 2.2 — Four-Point Bend Test Schematic

REGENERATOR CORE	RADIAL MOR KPa (PSI)		TANGENTIAL MOR KPa (PSI)		RADIAL COMPRESSION KPa (PSI)	
	B10	B50	B10	B50	B10	B50
CORE 1	372 (54)	606 (88)	1240 (180)	1964 (285)	152 (22)	255 (37)
CORE 2	613 (89)	758 (110)	1543 (224)	1915 (278)	310 (45)	393 (57)
CORE 3	379 (55)	482 (70)	1791 (260)	2170 (315)	310 (45)	413 (60)

Table 2.1 — Statistical Evaluation of Supplier A Sinusoidal AS Material (.061 mm Thick) Strength Data for Three Regenerator Matrices.

A Weibull failure distribution at a 90% confidence band was determined for each type of specimen using a Ford time-sharing library computer program. This program uses a least squares approximation if a statistically significant difference existed between the Weibull distributions for different cores. This program uses a two-sided test for significance at the 0.1% level.

The number of samples selected for the three matrix geometries was dependent on core availability. Since a relatively large number of full-size cores were received from Supplier A with the wrapped sinusoidal geometry fabricated from AS material (.061 mm thick), this structure was more fully characterized.

Specimens were cut from three different full-size cores to account for core-to-core variations. Table 2.1 lists the median B_{10} and B_{50} values of radial and tangential MOR and radial compression strength determined from a Weibull analysis of the failure data generated using the above specimens. Although the sample size is limited, it is evident from this data that the possibility exists of a fairly wide variation in material strength among several regenerator cores, as well as within a single core.

A statistically significant difference was detected in the radial compression data for Core 3 between those samples cut from the rim of the regenerator and the samples cut from the center of the core. Since past experience indicates that radial strength increases with decreasing core radius, the strength data presented here is based on the rim location samples.

A statistically significant difference was found to exist between the tangential MOR data for Core 1 and Core 3. In the radial direction, a statistically significant difference was found to exist in both the MOR and compression data between any two of the three cores. The compression specimens were observed to fail either in compression at a location several layers removed from the loaded surface, or in shear.

Significant differences in the Weibull distributions between cores would seem to be the result of processing variations rather than fundamental material property differences. In light of this, the Weibull distribution was determined for the aggregate data from the three cores to provide an estimate of the greatest range of strength that may be expected. This information is plotted in Figures 2.3 through 2.5 and the B_{10} and B_{50} values are listed in Table 2.2. The combined MOE data for the three A-S cores are plotted on Figures 2.6 and 2.7.

A statistical evaluation of the radial and tangential flexure strength and modulus was completed for the Supplier I extruded MAS matrix incorporating an isosceles triangular fin with a wall thickness of .135 mm (.0053 in). Since a full-size extruded regenerator had not been fabricated, test specimens were cut from 51 mm (2 in) square sample extrusions. For these samples, the radial direction was considered to be perpendicular to the matrix separator sheets. Weibull plots of the strength and modulus data are presented in Figures 2.8 thru 2.12. The B_{10} and B_{50} values are listed in Table 2.2. Since the extrusion process yields the most uniform geometric structure, the absence of a full-size extruded core should not be a detriment in the characterization of the physical properties for this matrix.

To characterize the structural integrity of the embossed square matrix fabricated by Supplier D with second generation MAS (MAS-2) material with a wall thickness of .193 mm (.0076 in.), specimens were taken from three different full-size cores. Weibull distribution for the aggregate data from the three cores for MOR and MOE are illustrated in Figures 2.13 to 2.17. The B_{10} and B_{50} values are listed in Table 2.2.

Once the physical properties and thermal expansion characteristics have been determined for each matrix geometry, thermal stress capacity can be estimated.

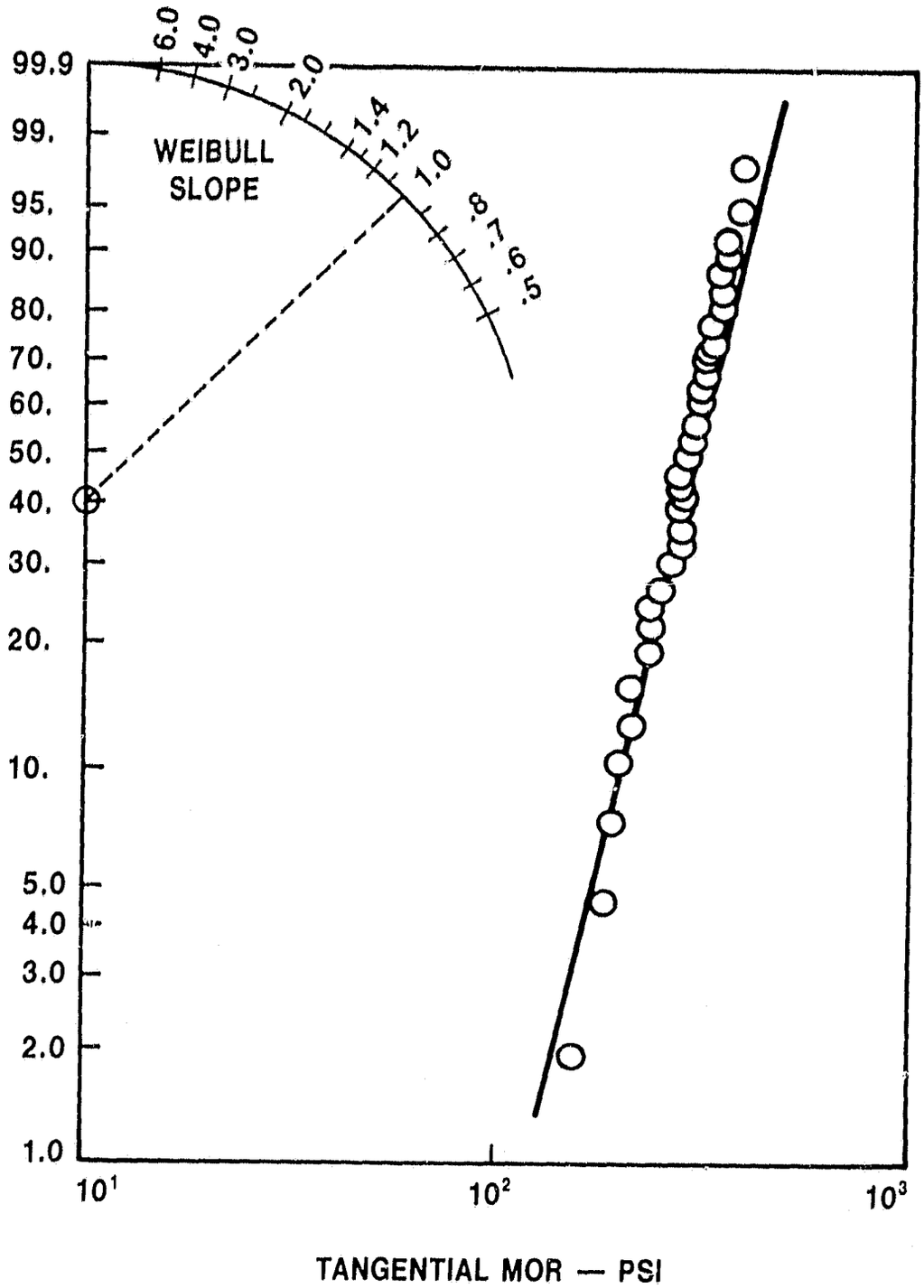

Figure 2.3 — Tangential Modulus of Rupture Distribution for Supplier A Sinusoidal AS Material (.061 mm Thick).

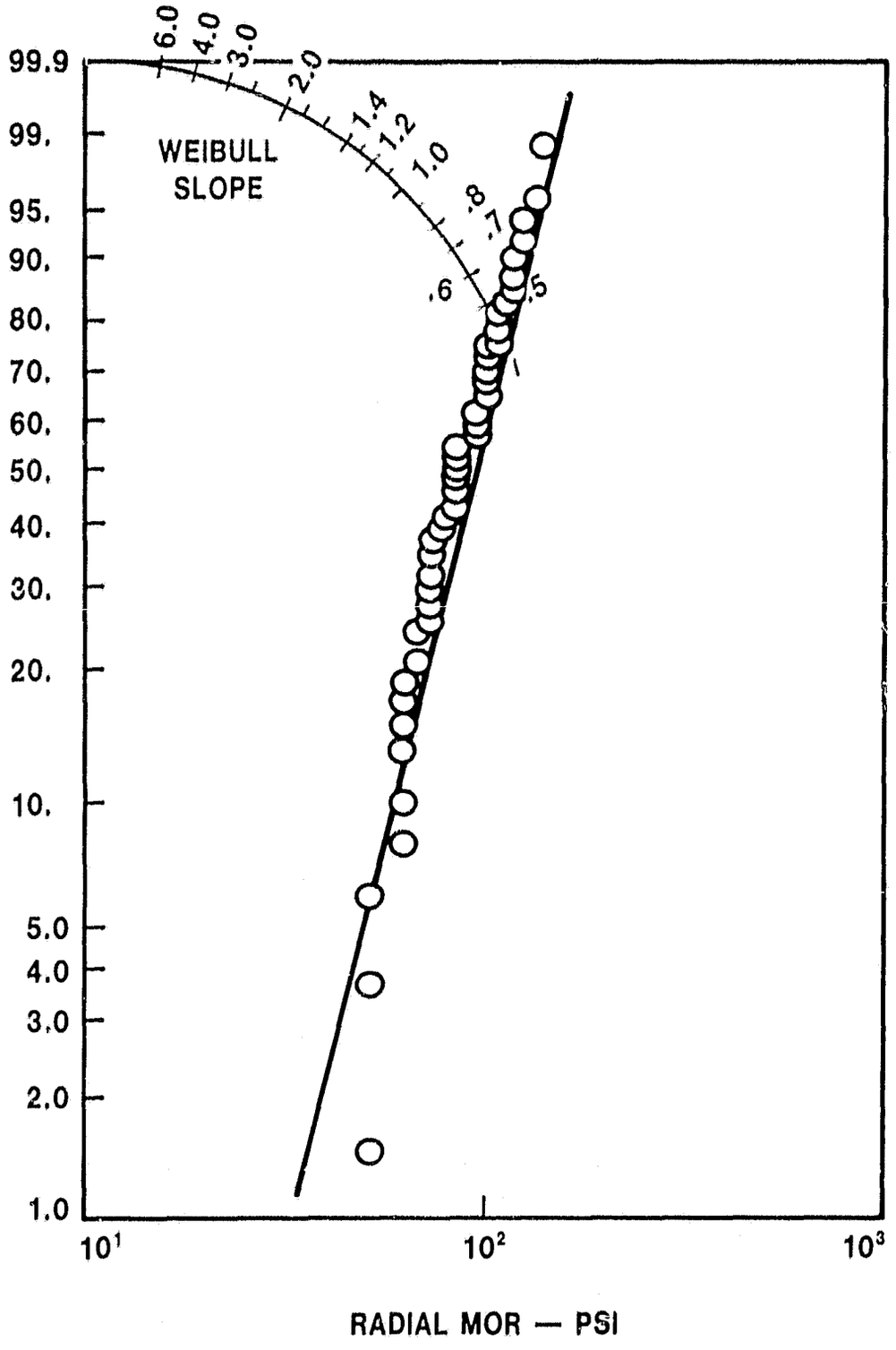

Figure 2.4 — Radial Modulus of Rupture Distribution for Supplier A Sinusoidal AS Material (.061 mm Thick).

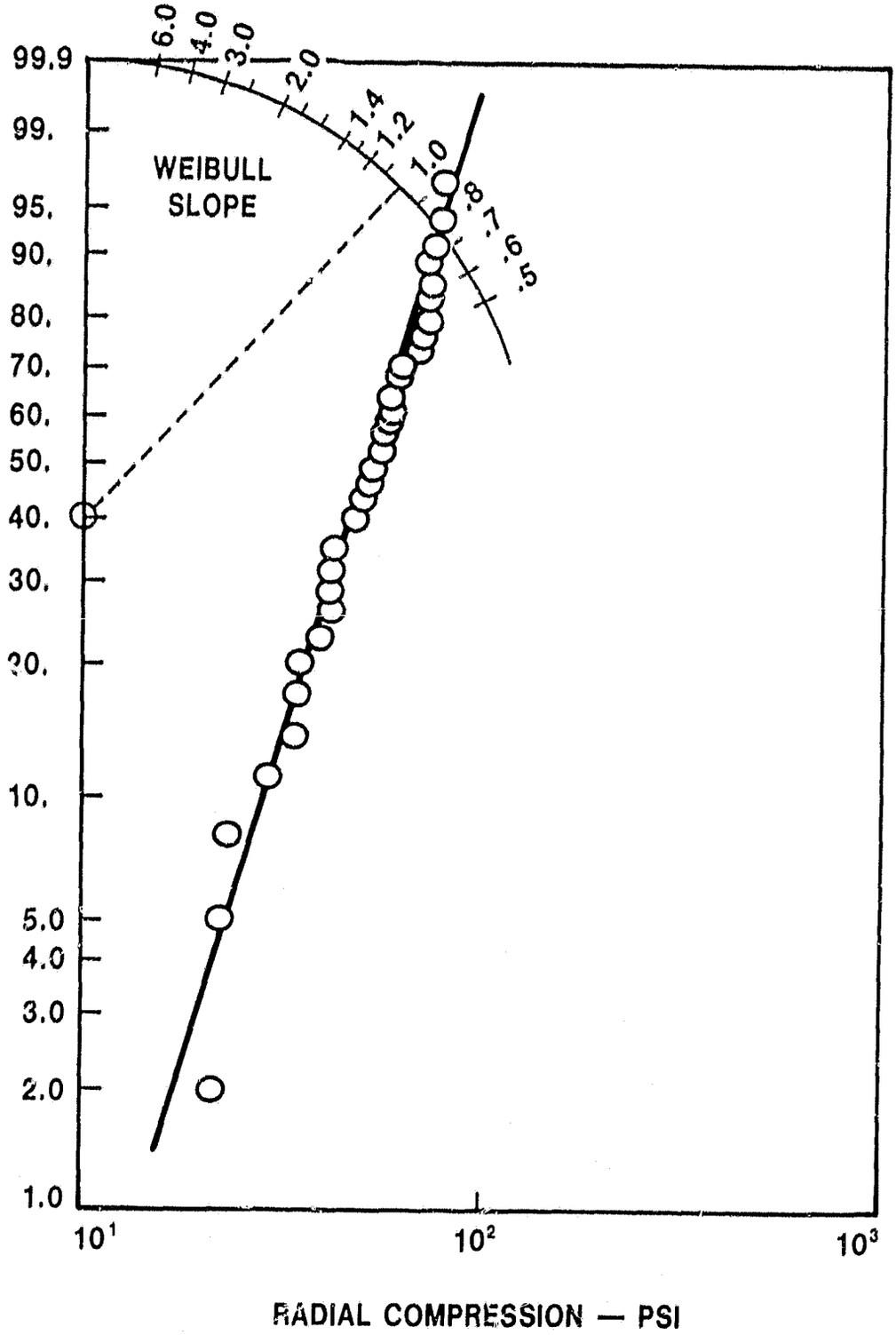

Figure 2.5 — Radial Compressive Strength Distribution for Supplier A Sinusoidal AS Material (.061 inm Thick).

CODE:

R — RECTANGULAR
I.T. — ISOSCELES TRIANGULAR
S.T. — SINUSOIDAL TRIANGULAR
H — HEXAGONAL
W — WRAPPED
C — CORRUGATED
EX — EXTRUDED
EM — EMBOSSED

MATRIX NO.	SUP-PLIER	MAT'L	MFG. PROCESS	TYPE OF FIN	X FINS/CM. (FINS/IN.)	Y ROWS/CM. (ROWS/IN.)	N HOLES/CM.^{2} (HOLES/IN.^{2})	S MM. (IN.)	B MM (IN.)	H MM. (IN.)	B_{50} MOR_T Kpa (PSI)	B_{10} MOR_T Kpa (PSI)	B_{50} MOE_T (X10^{-6}) Kpa (PSI)	B_{10} MOE_T (X10^{-6}) Kpa (PSI)	B_{50} MOR_R Kpa (PSI)	B_{10} MOR_R Kpa (PSI)	B_{50} MOE_R (X10^{-4}) Kpa (PSI)	B_{10} MOE_R (X10^{-4}) Kpa (PSI)	B_{50} $COMP_R$ Kpa (PSI)	B_{10} $COMP_R$ Kpa (PSI)	B_{10} ST_T (FPM)	B_{50} ST_T (FPM)	FPM @ 100°C	FPM @ 1000°C	ΔFPM	B_{10} θ	B_{50} θ
1	A	AS	W, C	S.T.	15.0 (38)	13.6 (34.5)	203.9 (1311)	.061 (.0024)	.061 (.0024)	.676 (.0266)	1998 (290)	1399 (203)	3.1 (.45)	2.14 (.31)	620 (90)	386 (56)	379 (.055)	193 (.028)	345 (50)	200 (29)	655	645	-30	200	230	2.85	2.80
2	I	MAS	EX	I.T.	15.8 (40)	9.1 (23)	142.6 (920)	.135 (.0053)	.135 (.0053)	.970 (.0382)	2274 (330)	1240 (180)	4.13 (.60)	3.38 (.49)	2274 (330)	1516 (220)	4.31 (.625)	4.07 (.59)	1688 (245)	1226 (178)	367	550	-20	1483	1530	24	37
3	D	MAS	W, EM	R	11.4 (29)	12.2 (31)	140 (900)	.193 (.0076)	.193 (.0076)	.627 (.0247)	2412 (350)	1654 (240)	6.75 (.98)	4.62 (.67)	1688 (245)	930 (135)	3.10 (.45)	2.34 (.34)	1309 (190)	944 (137)	358	357	20	1750	1730	21	21

Table 2.2 — Average Physical Properties for Three Regenerator Matrix Configurations.

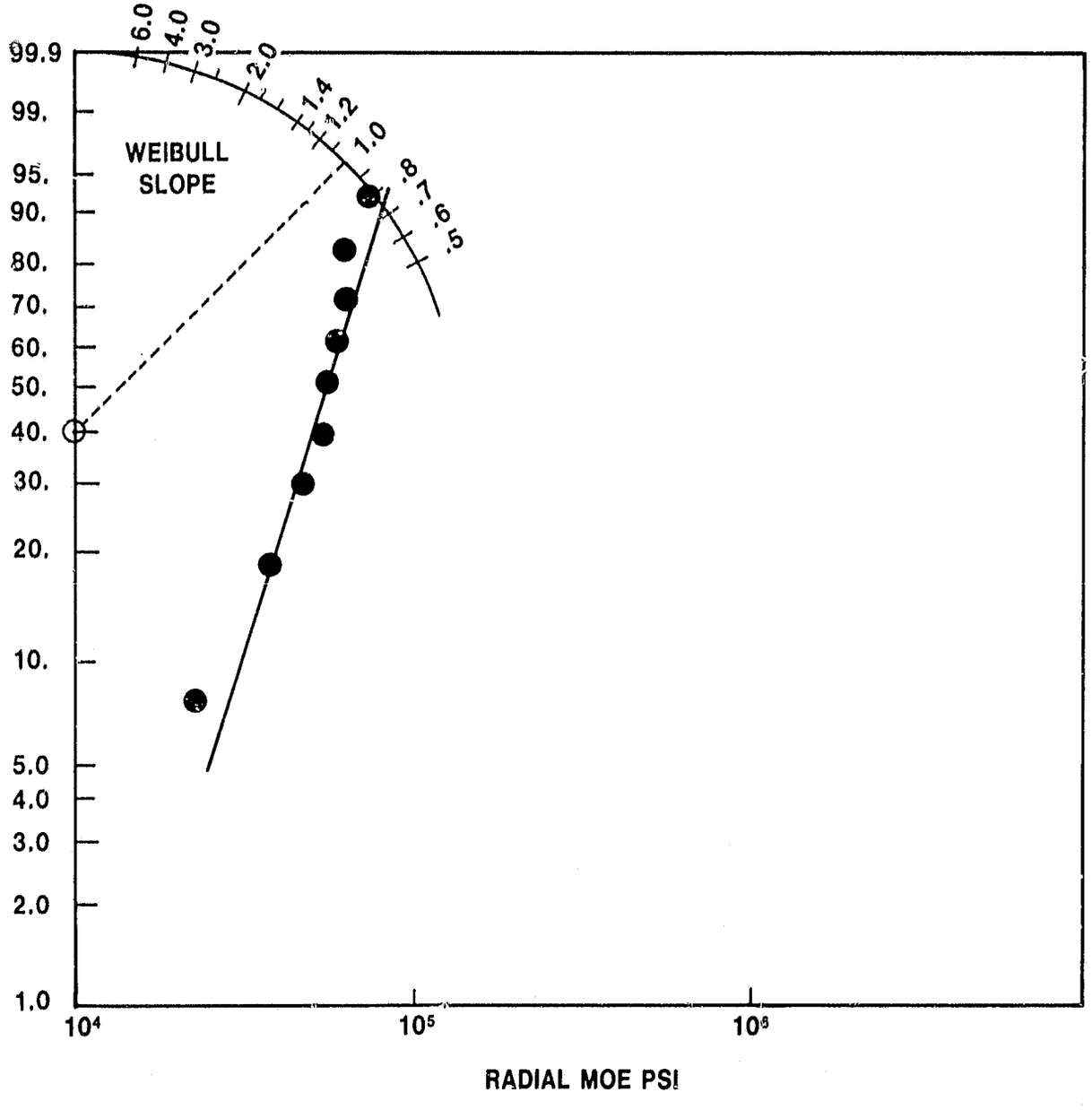

Figure 2.6 — Radial Modulus of Elasticity Distribution for Supplier A Sinusoidal AS Material (.061 mm Thick).

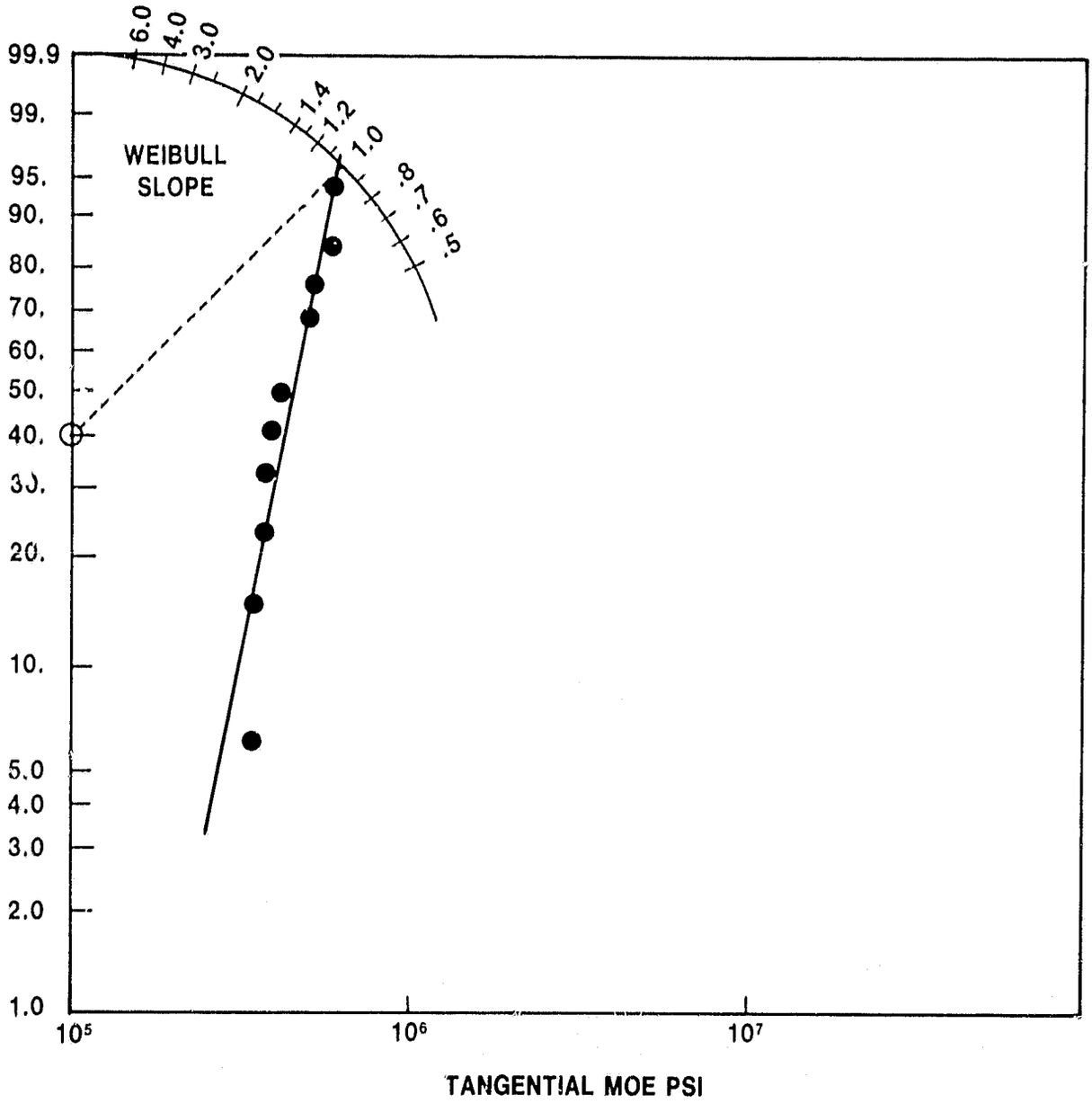

Figure 2.7 — Tangential Modulus of Elasticity Distribution for Supplier A Sinusoidal AS Material (.061 mm Thick).

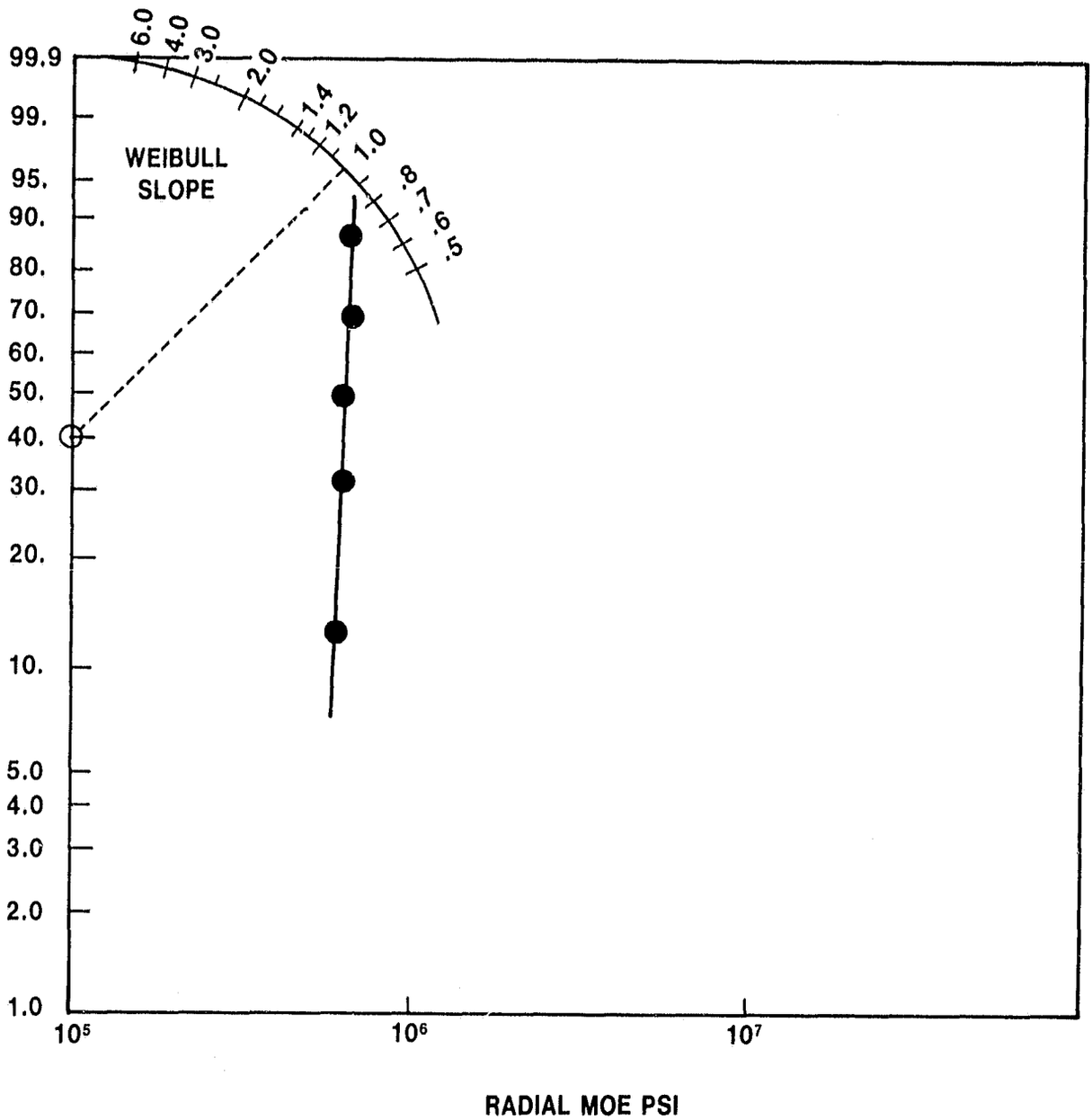

Figure 2.8 — Radial Modulus of Elasticity Distribution for Supplier I Isosceles Triangular MAS Material (.135 mm Thick).

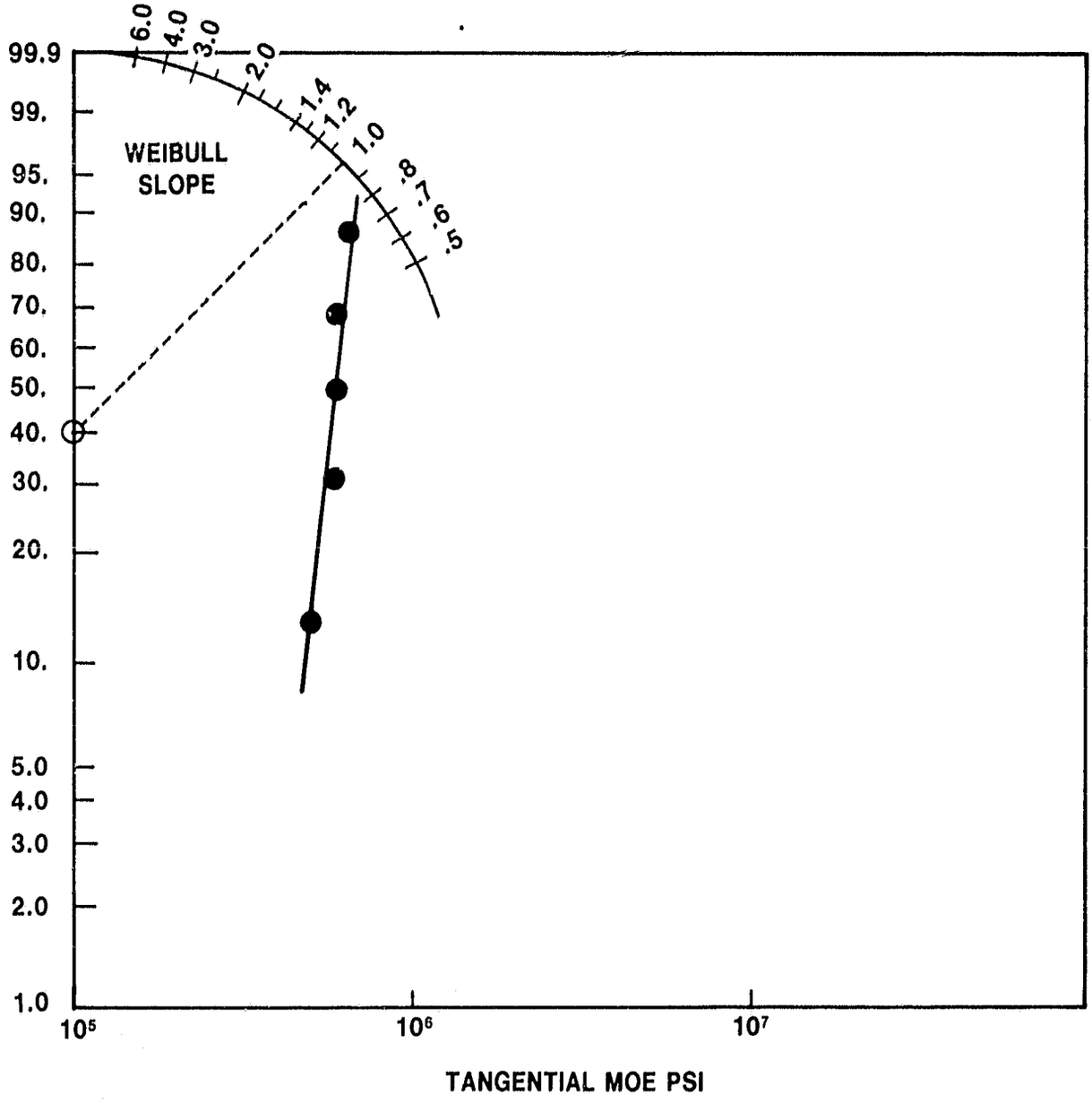

Figure 2.9 — Tangential Modulus of Elasticity Distribution for Supplier I Isosceles Triangular MAS Material (.135 mm Thick).

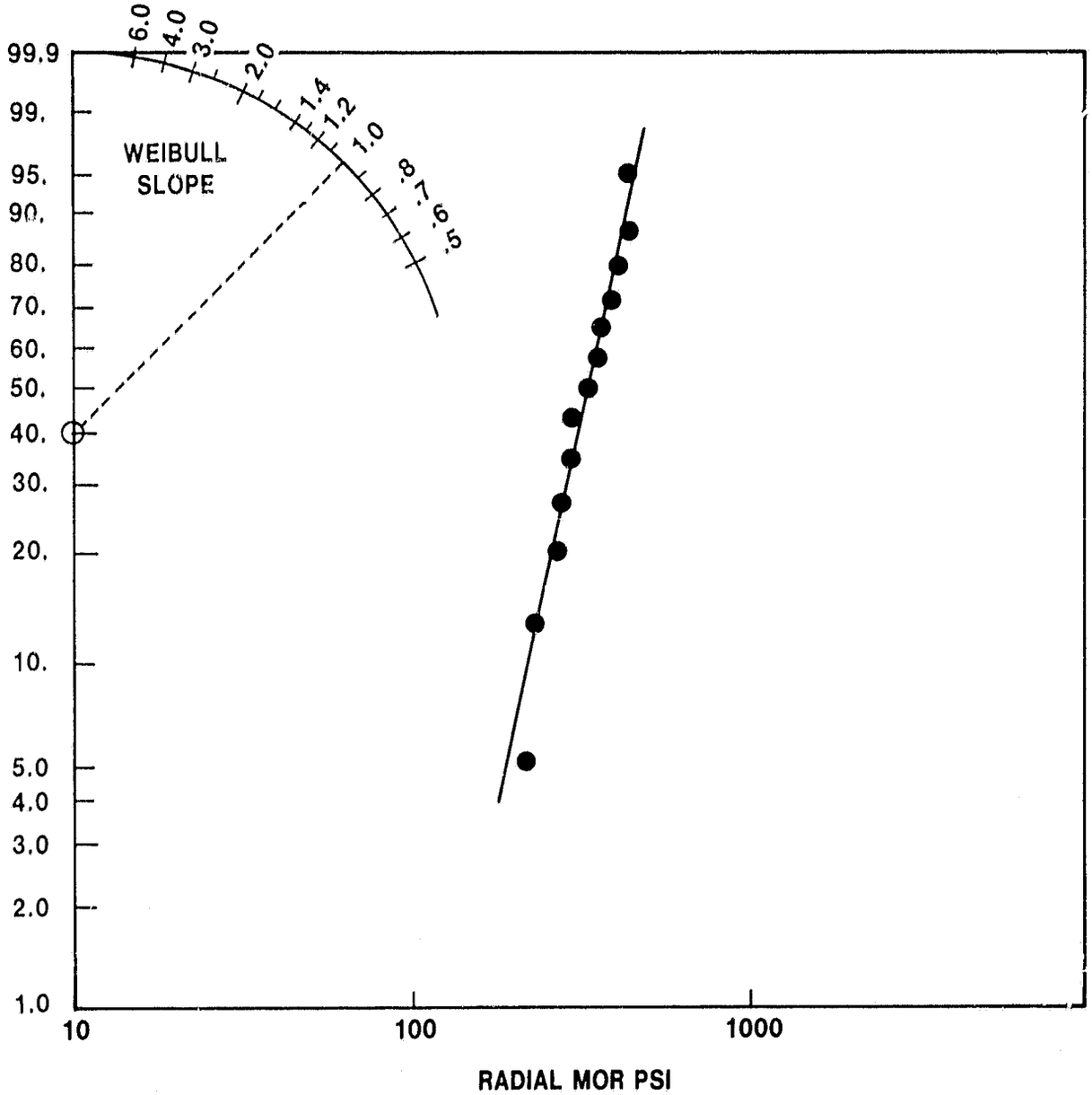

Figure 2.10 — Radial Modulus of Rupture Distribution for Supplier I Isosceles Triangular MAS Material (.135 mm Thick).

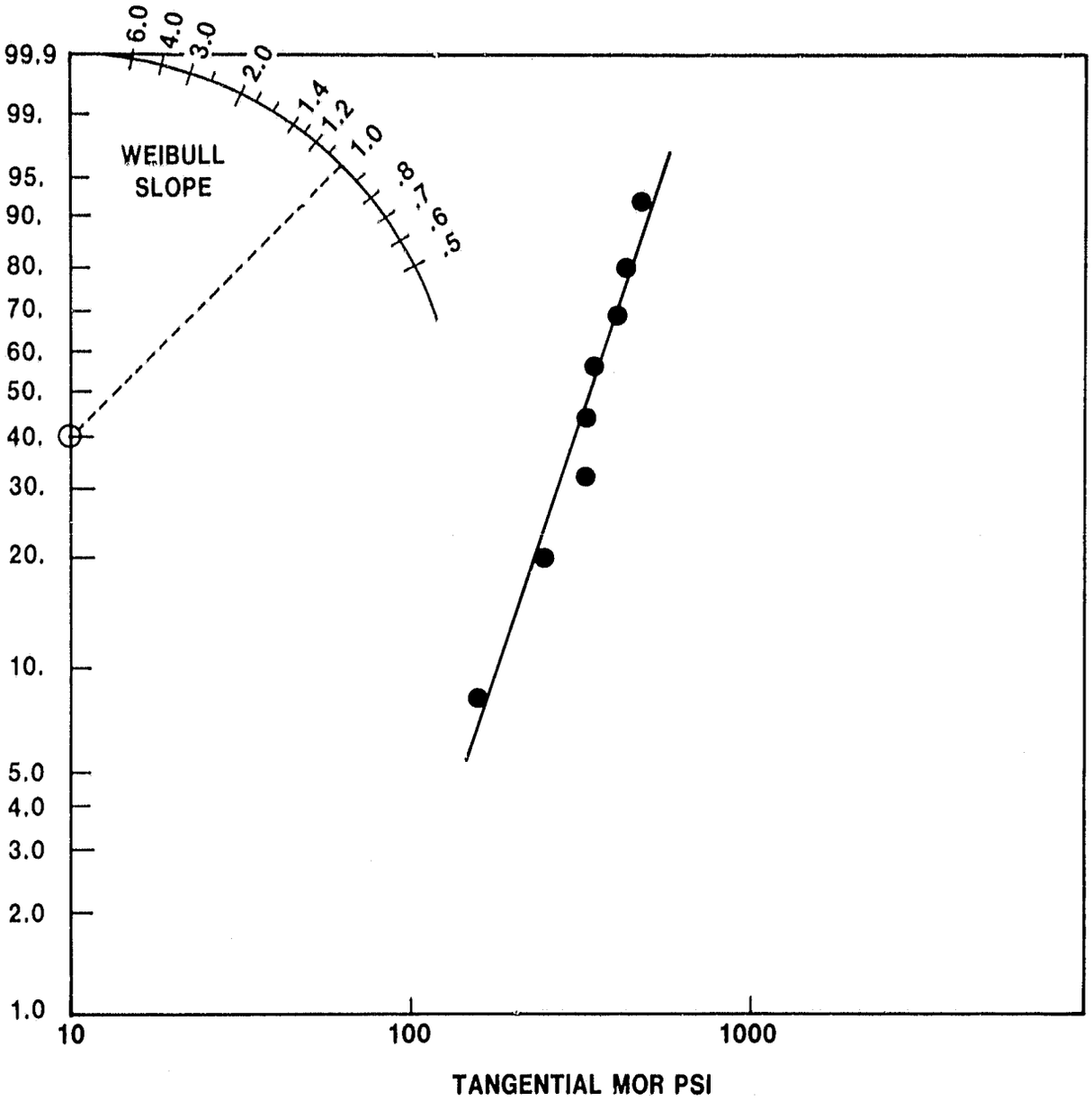

Figure 2.11 — Tangential Modulus of Rupture Distribution for Supplier I Isosceles Triangular MAS Material (.135 mm Thick).

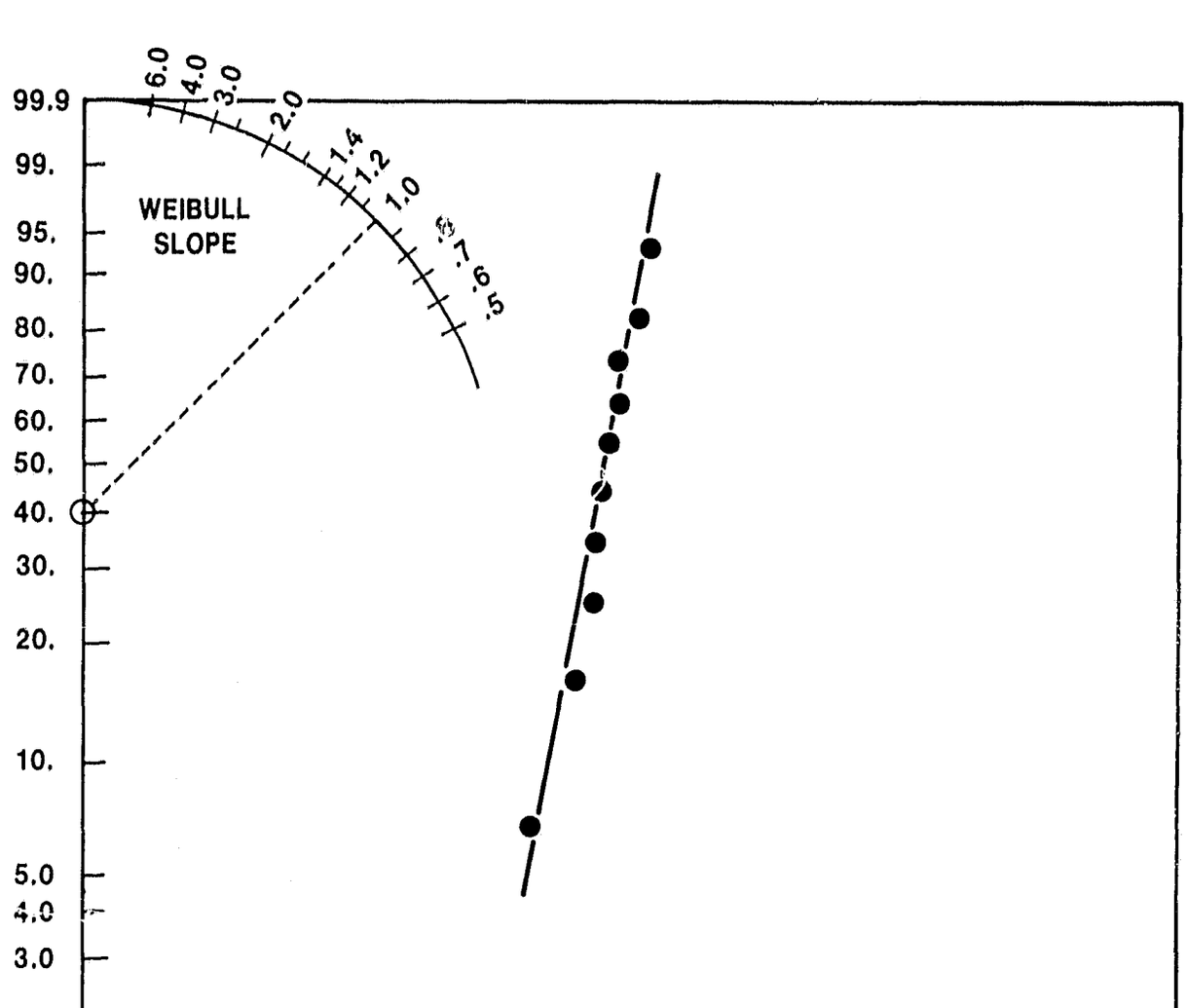

Figure 2.12 — Radial Compression Strength Distribution for Supplier I Isosceles Triangular MAS Material (.135 mm Thick).

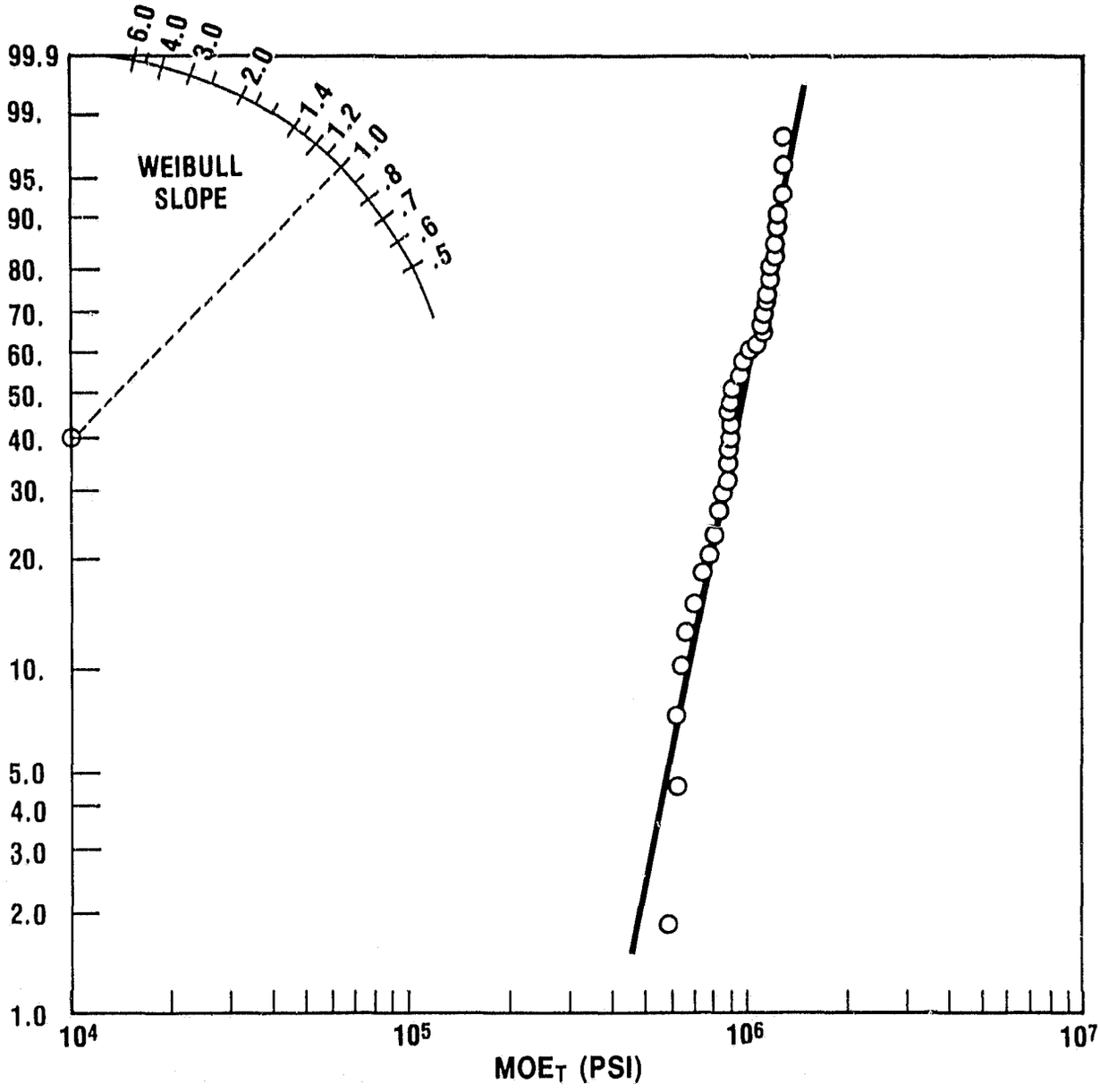

Figure 2.13 — Tangential Modulus of Elasticity Distribution for Supplier D Embossed Square MAS Material (.193 mm Thick).

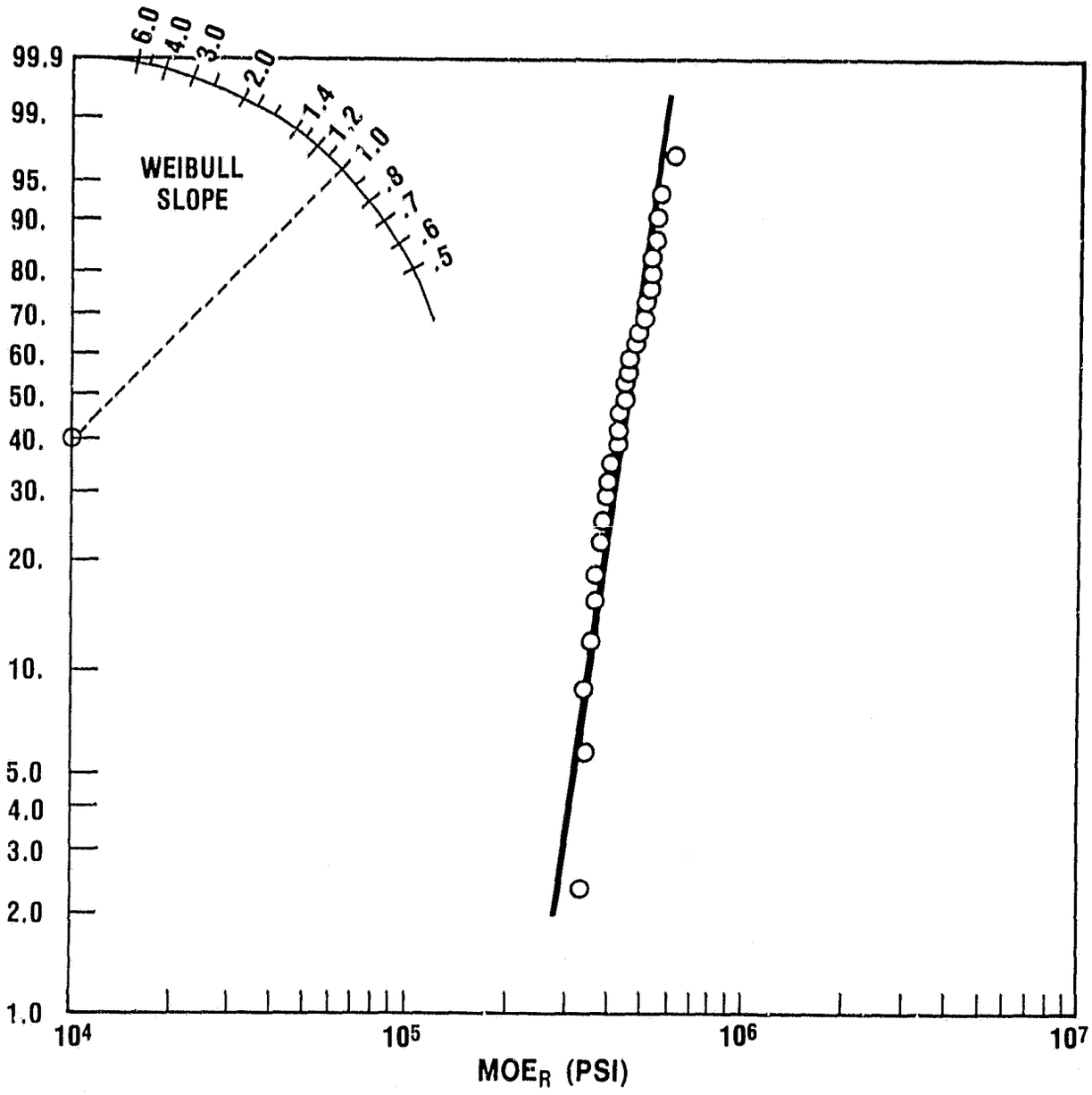

Figure 2.14 — Radial Modulus of Elasticity Distribution for Supplier D Embossed Square MAS Material (.193 mm Thick).

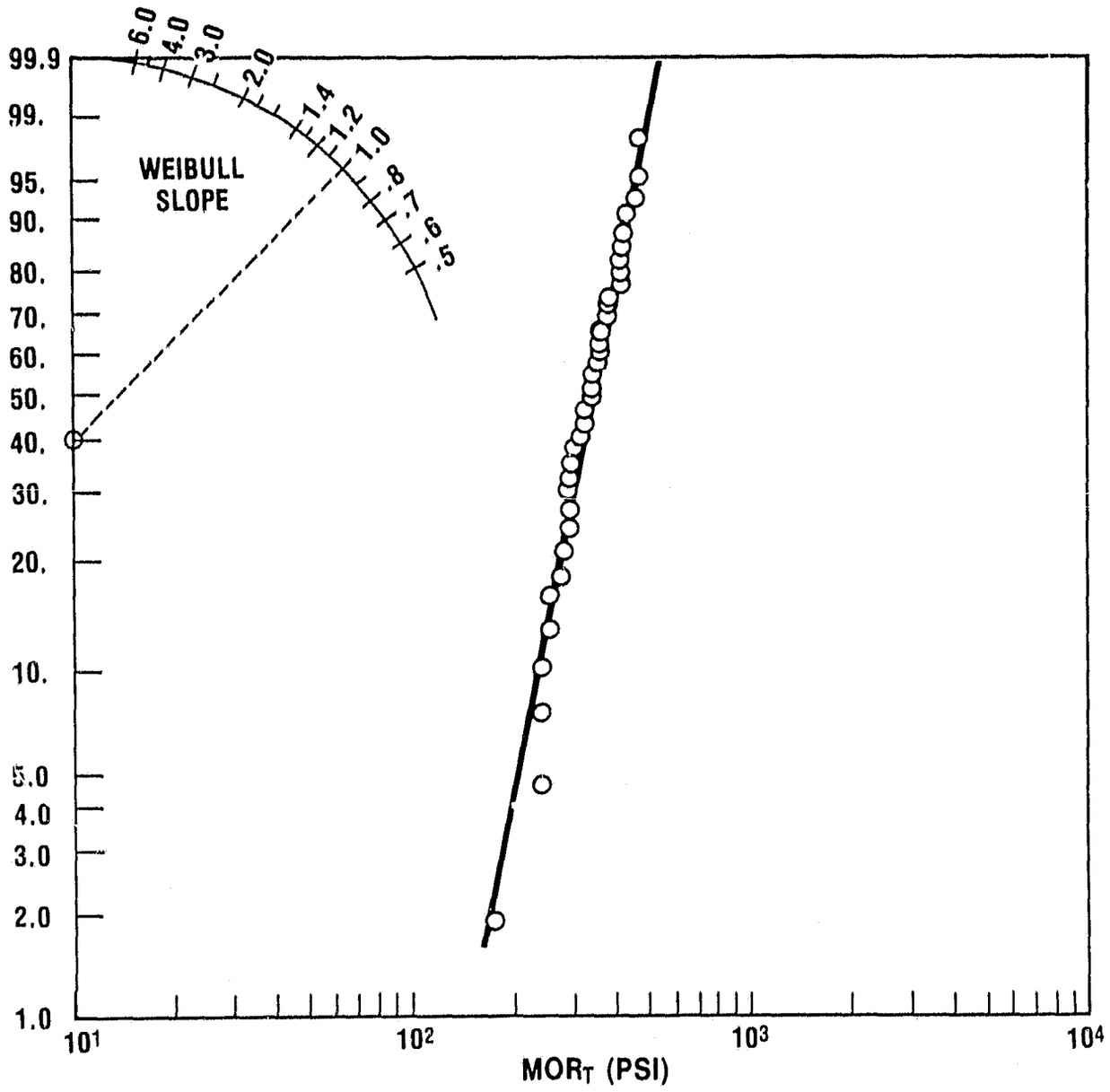

Figure 2.15 — Tangential Modulus of Rupture Distribution for Supplier D Embossed Square MAS Material (.193 mm Thick).

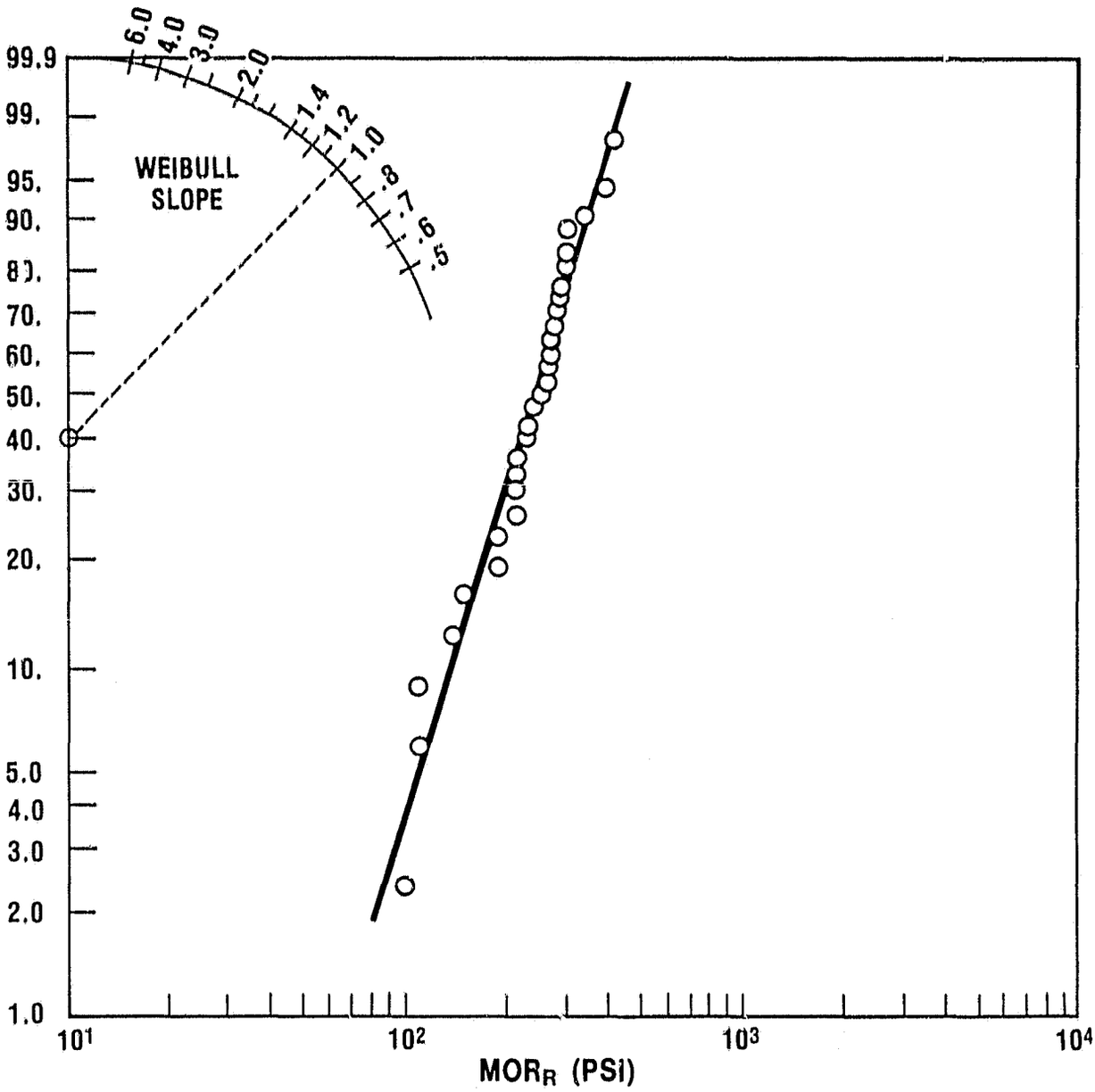

Figure 2.16 — Radial Modulus of Rupture Distribution for Supplier D Embossed Square MAS Material (.193 mm Thick).

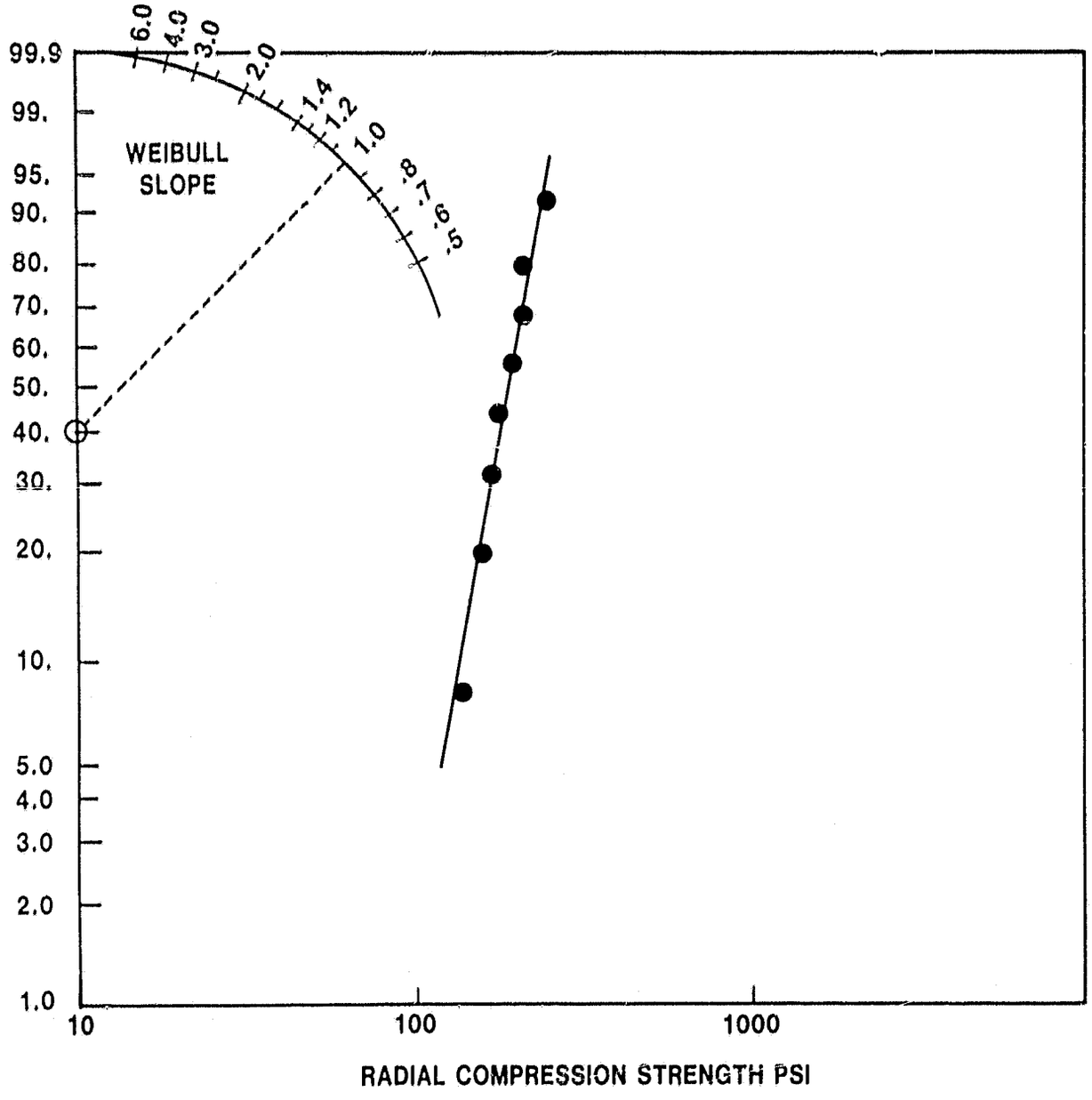

Figure 2.17 — Radial Compression Strength Distribution for Supplier D Embossed Square MAS Material (.193 mm Thick).

A dimensionless parameter that relates mechanical properties to thermal properties of the matrix is defined as the thermal stress factor (θ), which is the ratio of strain tolerance to the maximum expansion difference (ΔPPM) between the two temperature extremes of the regenerator. Strain tolerance (S.T.) is defined as the ratio of modulus of rupture to modulus of elasticity for the matrix. This parameter can be considered a relative measure of the intrinsic resistance of a matrix to thermal stress. Since the probability of thermal failure increases with decreasing thermal stress factor, it is a convenient criterion to compare and screen matrix materials on an equivalent basis. A large thermal stress factor indicates good resistance to thermal stress failure. A low thermal stress factor does not necessarily imply that the matrix material is not suited for a regenerator application. It does indicate that stress relief techniques may be required at the regenerator rim to provide sufficient thermal stress capacity.

For illustrative purposes the strain tolerance and thermal stress factor in the tangential direction for each matrix configuration are listed in Table 2.2 based on regenerator inlet temperatures of 100°C (212°F) and 1000°C (1832°F). Based on average values for thermal stress factors matrix 1 would not require rim stress relief, while matrix 3 would require more extensive stress relief compared to matrix 2. These premises are supported by engine durability results (reference 3).

3.0 RESISTANCE TO CHEMICAL ATTACK

The LAS (lithium aluminum silicate) family of materials have been found to be highly susceptible to chemical attack; otherwise these materials are ideally suited for regenerator use. The major cause of failure of early gas turbine regenerators was due to chemical attack of the LAS material (Ref. 1). The alkali lithium ions readily react with hydrogen ions from sulphuric acid in the engine exhaust and/or sodium ions found in the inlet air and exhaust gas. This type of reaction is commonly referred to as ion exchange since only the above mentioned ions interact whereas the aluminum and silicon ions and the oxygen anions which form the basic silicate open network structure (in this case a beta-spodumene solid solution structure) do not take part in the process.

The structure is affected by this reaction because the sodium or hydrogen ions are of different ionic sizes than the replaced lithium. The larger sodium ion causes the structure to expand and with the high regenerator surface area available for this reaction, increases in matrix bulk volume are observed. In addition, sodium increases the bulk thermal expansion of the matrix.

When the lithium ions interact with hydrogen ions the basic structure contracts since the latter is smaller in size. Bulk shrinkages of matrix specimens are observed at first with exposure to dilute sulphuric acid solutions. However, with continued exposure to dilute solutions, or with the use of more concentrated solutions, the material rapidly expands. When the matrix undergoes repeated exposures to sulphuric acid, thermal expansion is reduced when microcracking takes place.

The reason for this behavior can be found in the nature of the LAS polycrystalline microstructure. The individual crystallites are of the hexagonal structure with the thermal expansion defined by the a_0 and c_0 crystallographic axes. With LAS materials the difference in axial expansion coefficients is unusually high which leads to very large intergranular stresses in the polycrystalline compact. The increase in contraction of the structure as the hydrogen ion exchange proceeds, further increases the tensile stresses at the grain boundaries and microcracking at the boundaries occurs. The stored tensile strain energy in the microstructure resulting from cool down from the sintering temperatures is released in the process and bulk expansion of the matrix results even though the individual crystallites undergo a contraction.

In a full size LAS regenerator undergoing chemical attack in a gas turbine engine, changes in physical and thermal properties are manifested in two stages. First, the initially flat core will be observed to dish at room temperature. For instance, sodium attack at the hot face leads to convex dishing at this face resulting from the above mentioned growth. Sulphuric acid (hydrogen ions) attack at the cold face of the regenerator leads to convex dishings at this face resulting from the growth process attributed to the microcracking phenomenon discussed above. When the dishing has progressed to about .38-.65 mm (15-25 mils), mid-radius radial cracks will usually appear at the hot side surface and this is the second and more advanced stage of chemical attack.

For successful operation in a gas turbine regenerator application, a ceramic matrix material must be resistant to chemical attack.

Laboratory tests have been designed to evaluate the resistance of a ceramic matrix to attack by sodium and sulfur. Specifically, the tests are designed to promote sodium ion exchange and sulfuric acid leaching of the materials as may be experienced under engine operating conditions at the hot and cold face, respectively, of the regenerator core.

The cold face chemical attack test treats the materials to a 2 hour leaching in 1% sulfuric acid at ambient temperature. The specimens are then heated to 315°C (600°F), which approximates the turbine regenerator core cold face operating temperature, to promote H^+ — for-core-cation exchange. The degree of stability of the sample is discerned by measuring changes in sample length as well as changes in sample thermal expansion behavior between room temperature and 800°C (1472°F) as a result of a series of such chemical treatments.

The hot face chemical attack test provides a source of sodium ions for exchange with a host lattice cation by soaking the material in a 3.5% sodium chloride solution. The treated specimen is air dried for 2 hours at 200°C (392°F), fired at 800°C (1472°F), and stability (change in length) measurements are periodically carried out. The change in the material's thermal expansion behavior between room temperature and 800°C (1472°F) is also determined, as a significant change in this material characteristic is an indication of material instability.

It should be noted that the main purpose of these tests is to serve as a rough initial screening of candidate regenerator materials. The data is meaningful when it is compared to the baseline 9455 L·A·S material. Materials that exhibited an improvement when compared to the standard L·A·S materials were then fabricated into full-size cores, for a more complete evaluation in the 707 engine.

The results of the cold face chemical attack test are illustrated in Figure 3.1 for the three matrix structures as compared to the standard 9455 L·A·S material, which was utilized in the production 707 Ford gas turbine engine. Compared to the standard L·A·S material the stability of the A·S and M·A·S materials is significantly better after four test cycles.

Past experience has indicated that four test cycles is sufficient to establish the stability pattern for this initial screening test.

Figure 3.2 depicts the thermal expansion characteristics of these materials before and after the exposure to sulphuric acid. The 9455 L·A·S standard, which exhibits significant growth under the cold face test conditions (Figure 3.1), has undergone some pronounced changes in thermal expansion behavior (Figure 3.2). The A·S material exhibits negligible change in physical stability and expansion at 800°C (1472°F). This is not surprising in lieu of the absence of lithium in this material. The growth experienced by both M·A·S materials under cold face test conditions was accompanied by a lower thermal expansion behavior after testing. While not as stable as the A·S material, the M·A·S materials demonstrated enough of an improvement compared to the standard L·A·S material, to warrant further investigation as a full-size core under actual engine conditions.

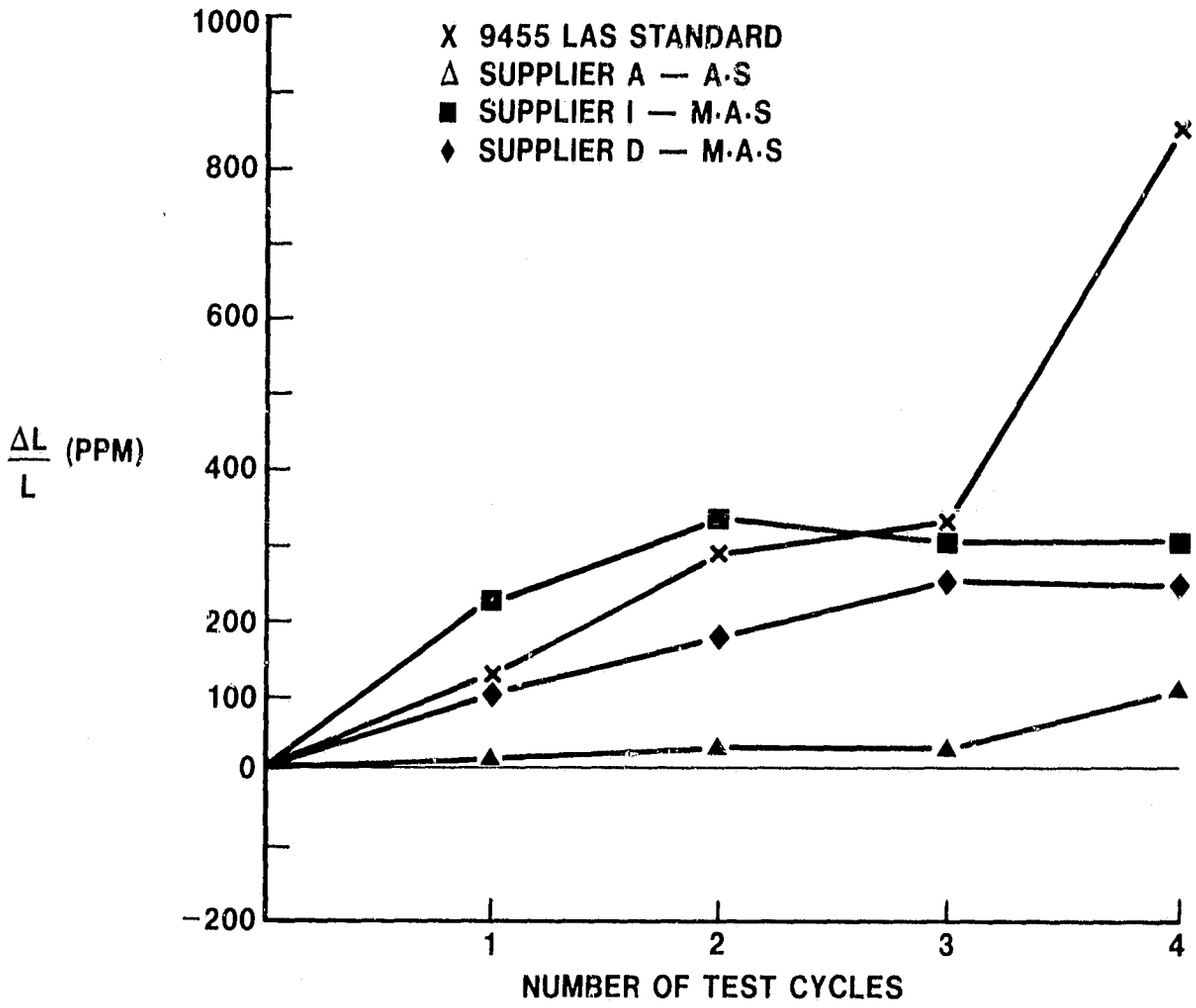

Figure 3.1 — Physical Stability of Various Materials After Exposure to Sulphuric Acid Simulating Cold Face Regenerator Test Conditions

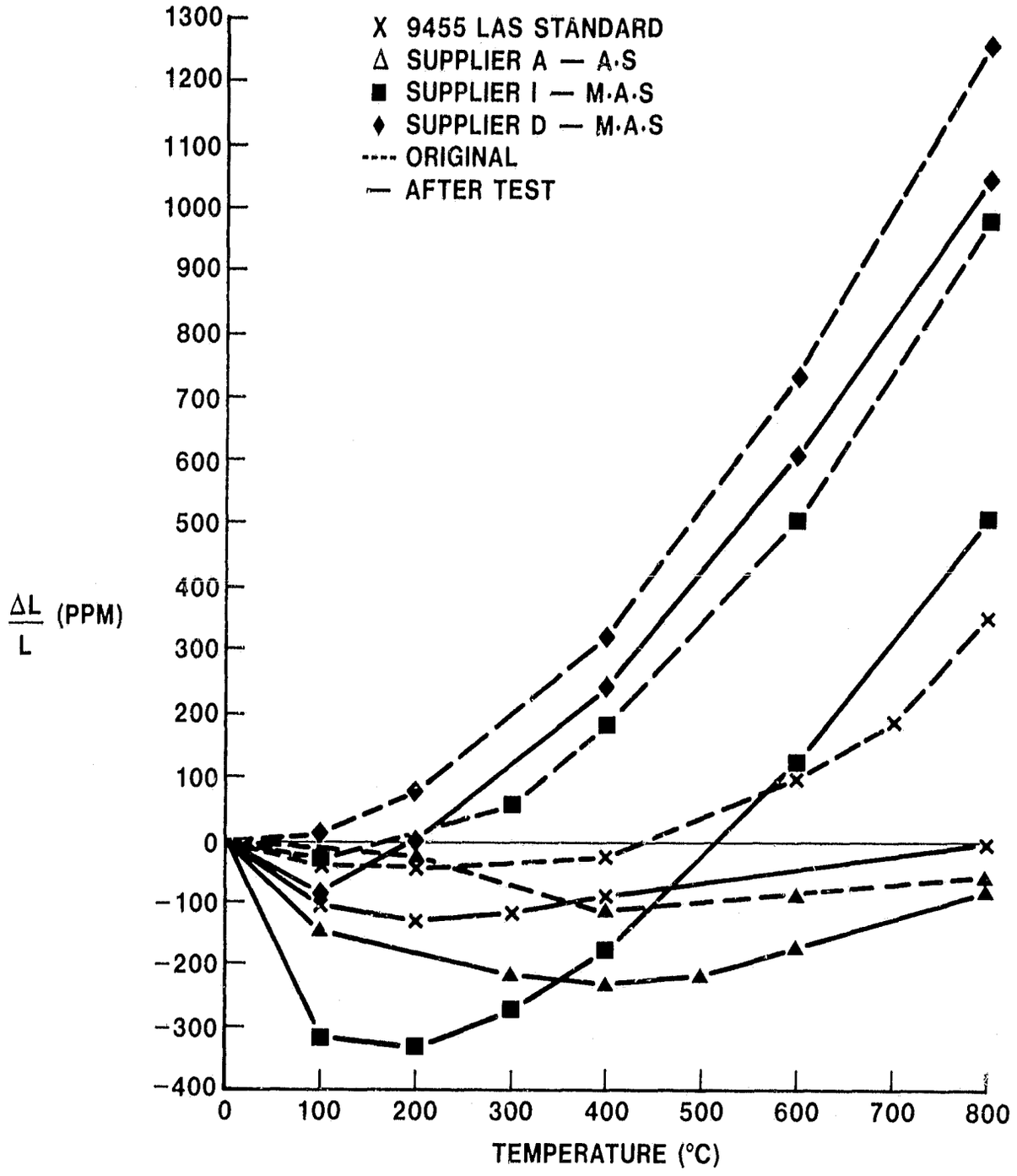

Figure 3.2 — Matrix Thermal Expansion Before and After Exposure to Sulphuric Acid Simulating Cold Face Regenerator Test Conditions

The physical stability of these materials under hot face test conditions (Figure 3.3) shows improved resistance to sodium attack at 800°C (1472°F) compared to the 9455 L·A·S standard. Each of the materials experience an immediate and significant reaction to the elevated sodium treatment, followed by subsequent periods of virtual stability. The exception is the 9455 L·A·S material, which undergoes a consistent increase in dimensional change. For the A·S and M·A·S materials the initial sodium intrusion into these materials may form a boundary zone through which further penetration is slowed. The diffusion of sodium from this boundary zone into adjacent, pristine material would then become the rate-controlling step. The progress of this diffusion, causing modification of the sodium ion concentration and the establishment of a gradient in the near-surface zone of exchange, could reactivate a subsequent utilization of surface sodium.

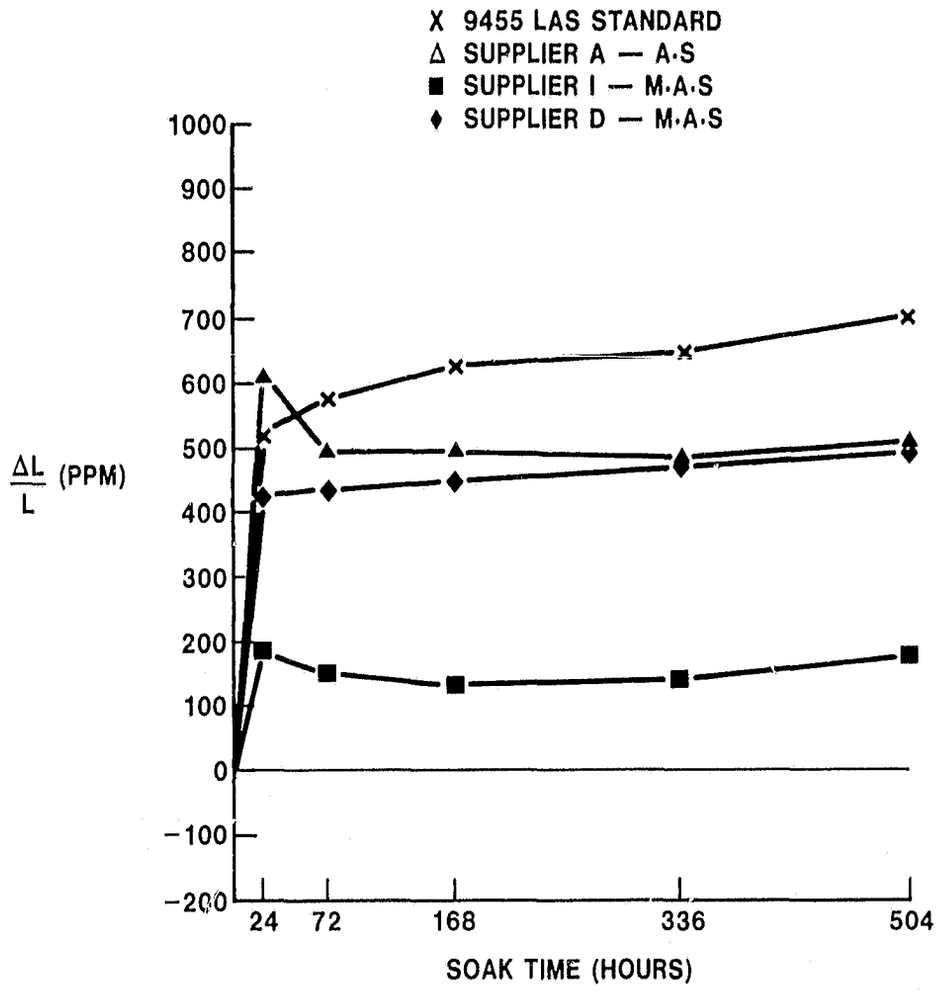

Figure 3.3 — Physical Stability of Various Materials After Exposure to Sodium Simulating Hot Face Regenerator Test Conditions

Figure 3.4 displays the thermal expansion behavior of the A·S and M·A·S materials and the 9455 LAS standard before and after hot face testing. A comparison of these figures, using the hot face test data of Figure 3.3 as a reference, provides an insight into the changes experienced by these materials during their exposure to the laboratory test conditions designed to simulate the hot face of a gas turbine regenerator.

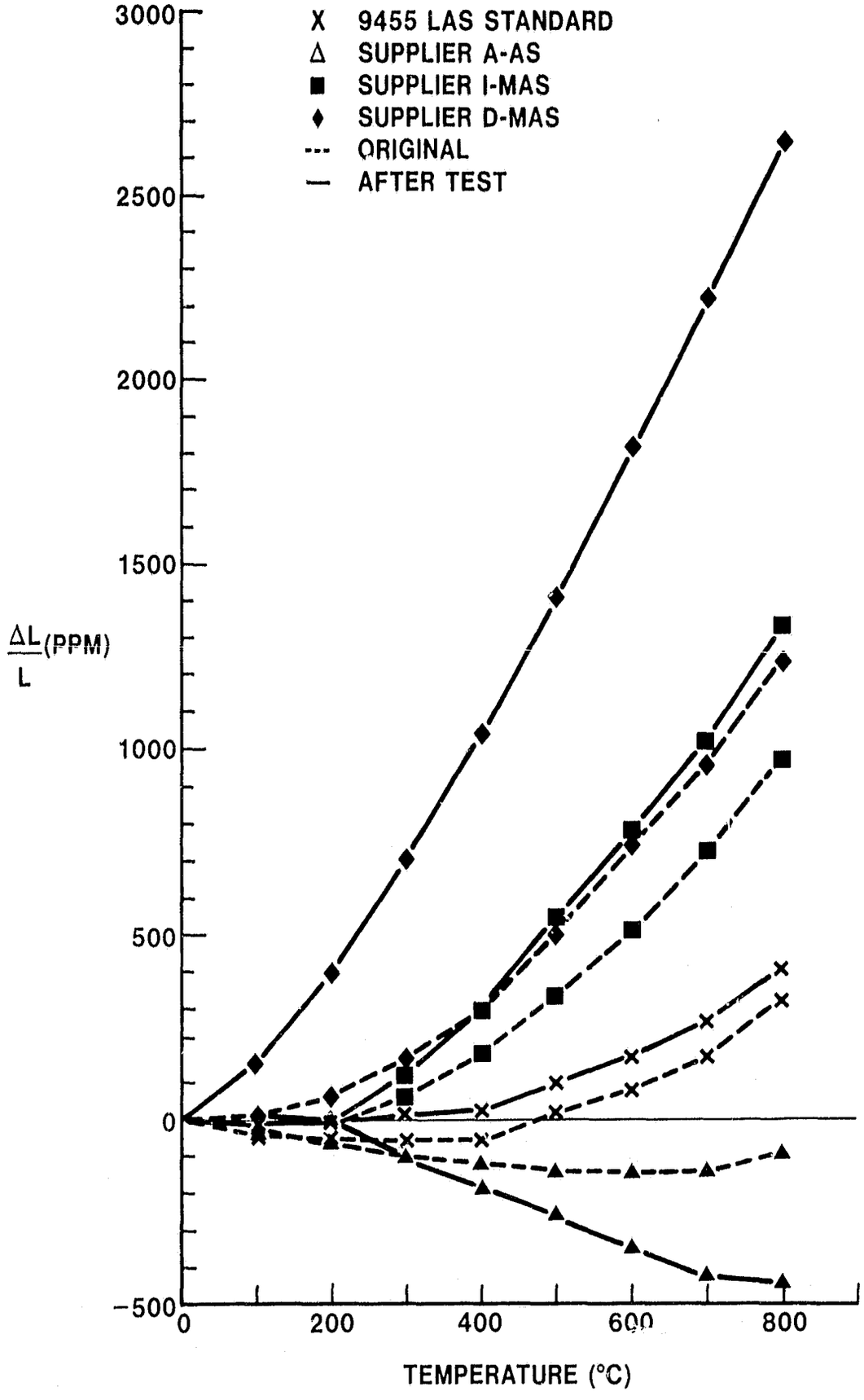

Figure 3.4 — Thermal Expansion Before And After Exposure to Sodium Simulating Hot Face Regenerator Test Conditions

The 9455 L·A·S standard experienced a mild elevation in thermal expansion behavior, but the basic character of the material response to temperature change was not modified. After testing, the A·S material became more strongly contractive with increasing temperature. The M·A·S materials exhibited a correspondingly greater perturbation in their thermal expansion behavior (Figure 3.4) proportionate to their hot face test growth (Figure 3.3). This is suggestive of a microcracking type of damage phenomenon. Of interest is the observation that both of the M·A·S materials experienced a change in thermal expansion in the opposite direction to that of the cold face testing.

In summary the A·S and M·A·S materials exhibited improved dimensional stability when compared to the 9455 LAS standard for both the cold face (Figure 3.1) and hot face (Figure 3.3) testing. The thermal expansion behavior after exposure to sulphuric acid (Figure 3.2) and sodium (Figure 3.4) at 800°C (1472°F) is inconclusive. It should be noted that these tests serve only as a coarse screening method to evaluate materials for resistance to chemical attack when compared to L·A·S. The expected improvement in dimensional stability exhibited by the A·S and M·A·S materials in the physical stability data (Figures 3.1 and 3.3) was later verified in engine testing of full-size cores (Reference 3).

4.0 THERMAL STABILITY

To increase engine efficiency, designers propose higher operating temperatures for the alternate heat engines of the future. This, in turn, places greater thermal demands on the regenerator core. In anticipation of these elevated temperature requirements, the thermal stability testing program is designed to systematically test materials, with and without corrosive agents present, over the temperature range of 1000°C (1832°F) to 1200°C (2192°F). Thus, thermal stability testing will serve to place upper temperature limits on the serviceability of present generation matrix materials (aluminous silicate and magnesium aluminum silicate). This high temperature testing was carried out, both with and without sodium present, at temperatures of 1000°C (1832°F), 1100°C (2012°F) and 1200°C (2192°F).

The high temperature dimensional stability of the A·S and M·A·S materials was evaluated by periodic measurements of specimen length change as a function of time held at the test temperature. The thermal expansion behavior between room temperature and the test temperature was determined for each material before testing and after completing the prescribed testing schedule. The procedure used to evaluate the high temperature dimensional stability of a material in the presence of sodium is identical to the above-described procedure, except that the samples were treated prior to the testing program with a sodium-bearing material. This was accomplished by soaking in a 3.5% sodium chloride solution. A comparison of the data from both tests will point out the propensity of these ceramic materials to suffer corrosion by sodium at these elevated temperatures. As in previous testing, all length measurements are determined using a Sheffield Visual Comparator with 5000:1 amplification. Lengths are measured and reported to the nearest 2.5×10^{-5} mm (one millionth of an inch), and the measurement is reported to be accurate to within $\pm 1.30 \times 10^{-4}$ mm (±5 millionths of an inch). During the heating to and cooling from the test temperature, rates of less than 50°C (90°F) per minute are maintained in order to eliminate any dimensional changes induced by thermal shock.

The high temperature dimensional stability testing for the 9455 L·A·S standard, A·S and M·A·S materials were evaluated for a maximum 1008 hour exposure at 1000°C, 1100°C and 1200°C with and without sodium present. The total change in specimen length after this exposure at the three temperature levels is tabulated in Table 4.1, with and without the presence of sodium. The change in thermal expansion after exposure (1008 hours max.) at each of the test temperatures with and without sodium is listed in Table 4.2. Each material can be evaluated by comparing the dimensional change (Table 4.1) and thermal expansion behavior (Table 4.2) at each of the test temperatures.

The data indicates the standard 9455 L·A·S material is quite stable without sodium present (Table 4.1 & 4.2). As expected in the presence of sodium the dimensional change (Table 4.1) and thermal expansion characteristics (Table 4.2) have increased significantly. This trend establishes a baseline for comparison for the A·S and M·A·S materials.

The Supplier A·A·S material appears to be temperature limited to 1000°C. Although the change in length (Table 4.1) and expansion (Table 4.2) is within accept-

able limits at 1000°C, the drastic increase in both parameters terminated the testing at higher temperatures prior to the 1008 hour objective. The presence of sodium appeared to have little effect on both parameters. It should be noted that over 30,000 hours on a sample of eight cores of this material were accumulated in the Ford 707 gas turbine at 1000°C (1472°F) inlet temperature. Four cores exceeded 5000 hours with a maximum of 8000 + hours. This experience substantiates the acceptability of the dimensional change (450 to 600 ppm) observed in the laboratory testing at 1000°C.

		DIMENSIONAL CHANGE AFTER 1008 HOUR EXPOSURE (PPM)					
		WITHOUT SODIUM			WITH SODIUM		
SUPPLIER	MATERIAL	1000°C	1100°C	1200°C	1000°C	1100°C	1200°C
A	9455 L·A·S (STANDARD)	− 80	−120	−300	1220	550	800
A	A·S	−450	−2250 (672 HRS)		− 600	−3070 (168 HRS)	−9190 (168 HRS)
I	M·A·S	− 80	400	800	300	600	1050
D	M·A·S	− 50	−100	−200	400	275	− 400

Table 4.1 — Matrix Dimensional Change After 1008 Hour Exposure At Test Temperature With and Without Sodium Present

		INITIAL PPM AT TEST TEMPERATURE			FINAL PPM AT TEST TEMPERATURE AFTER 1008 HR. EXPOSURE					
					WITHOUT SODIUM			WITH SODIUM		
SUPPLIER	MATERIAL	1000°C	1100°C	1200°C	1000°C	1100°C	1200°C	1000°C	1100°C	1200°C
A	9455 L·A·S (STD)	650	750	1050	725	800	1125	1000	1000	1300
A	A·S	40	100	200	280	930 (672 HRS)		400	1100 (168 HRS)	4100 (168 HRS)
I	M·A·S	1480	1750	2400	1380	1425	1550	1380	1500	1200
D	M·A·S	1800	1950	2250	2100	2025	2500	2100	2200	2300

Table 4.2 — Matrix Thermal Expansion At Test Temperature After 1008 Hour Exposure With and Without Sodium Present

Samples of a second generation A·S material have recently been received from Supplier A. This material is expected to have acceptable thermal stability up to 1100°C. Laboratory evaluations have been initiated in order to provide confirmation.

The dimensional change (Table 4.1) and thermal expansion characteristics (Table 4.2) of the Supplier D-MAS materials throughout the temperature excursion indicates excellent stability for this material. The presence of sodium had minor effects on both parameters. This material achieved almost 500 hours in the Ford 707 engine at 1000°C inlet temperature without any discernible effects.

Based on thermal expansion data (Table 4.2) the presence of sodium appears to have negligible effect on the Supplier I-MAS material. While not as stable as the

Supplier D-MAS material, the Supplier I-MAS material does exhibit good dimensional stability (Table 4.1) up to 1100°C. Although the increase in length is more pronounced at 1200°C this material is still a viable candidate at this temperature. Full-size cores of this material were received during the late stages of the NASA/Ford ceramic regenerator systems development program. No apparent difficulties were encountered after 2500 and 250 hours at 800°C and 1000°C, respectively.

Correlation with full-size cores evaluated under actual engine conditions adds credence to the true value of controlled laboratory test procedures. The actual value for dimensional change and alterations in thermal expansion characteristics from laboratory tests are inconclusive on a singular basis for each material. But when compared collectively to a standard material, which has an established durability potential in an actual engine environment, an insight into the preliminary durability potential of candidate regenerator materials can be gained before the fabrication of full-size cores. The final durability potential must ultimately be determined under actual engine conditions.

ACKNOWLEDGEMENTS

The author wishes to acknowledge the significant contributions of Mr. J. A. Cook, Mr. J. N. Lingscheit and Mr. V. D. N. Rao toward the information presented in this report.

REFERENCES

1. Anderson, D. H., Fucinari, C. A., Rahnke, C. J., and Rossi, L. R., Annual Summary Report, No. 2630-1, Automotive Gas Turbine Ceramic Regenerator Design and Reliability Program, ERDA Contract No. E (11-1) 2630, Sept. 15, 1975.

2. Cook, J. A., Fucinari, C. A., Lingscheit, J. N., and Rahnke, C. J., Annual Summary Report, No. 2630-18, Automotive Gas Turbine Ceramic Regenerator Design and Reliability Program, ERDA Contract No. E (11-1) 2630, Oct. 15, 1976.

3. Fucinari, C. A., Rahnke, C. J., Rao, V. D. N., and Vallance, J. K., Ceramic Regenerator Systems Development Program — Final Report, NASA CR- , NASA Contract No. DEN 3-8, June, 1980.

4. C. P. Howard, "Heat Transfer and Flow Friction Characteristics of Skewed Passage and Glass-Ceramic Heat Transfer Surfaces", T. R. No. 59, Department of Mechanical Engineering, Stanford University, Oct. 1963.

1. Report No NASA CR-159854	2. Government Accesnion No	3. Recipient's Catalog No
4. Title and Subtitle Regenerator Matrix Physical Property Data		5. Report Date May, 1980 6. Performing Organization Code
7. Author(s) C. A. Fucinari		8. Performing Organization Report No 10. Work Unit No.
9. Performing Organization Name and Address Research Staff Ford Motor Co. Dearborn, Michigan 48121		11. Contract or Grant No. Den 3-8
12. Sponsoring Agency Name and Address U.S. Department of Energy Office of Transportation Programs Washington, D. C. 20545		13. Type of Report and Period Covered Contractor Report 14. Sponsoring Agency Report No. DOE/NASA/0008-80/11

15. Supplementary Notes

Topical Report. Prepared under Interagency Agreement EC-77-A-31-1044, Project Manager, Thomas J. Miller, Transportation Propulsion Division, and Dr. Thomas P. Herbell, Materials Division, NASA Lewis Research Center, Cleveland, Ohio 44135

16. Abstract

This report will compile the key physical and thermal property data for a limited number of matrix configurations. These data will include heat transfer and pressure drop characteristics, compressive strength, tensile strength and elasticity, thermal expansion characteristics, chemical attack, and thermal stability test results.

17. Key Words (Suggested by Author(s))	18. Distribution Statement
Heat Exchangers Ceramic Regenerator Systems Ceramic Materials Heat Exchanger Manufacturing	Unclassified — unlimited STAR Category 85 DOE Category UC-96

19. Security Classif. (of this report)	20. Security Classif. (of this page)	21. No. of Pages	22. Price*
Unclassified	Unclassified	50	

*For sale by the National Technical Information Service, Springfield, Virginia 22161

NASA-C-168 (Rev. 10-75)